Li-ion Battery Electrode State of Charge and Degradation Monitoring Using Battery Casing as the Reference Electrode

by

MD ASHIKUR RAHMAN

A thesis submitted to the
School of Graduate and Postdoctoral Studies in partial
fulfillment of the requirements for the degree of

Master of Applied Science in Mechanical Engineering

Department of Automotive and Mechatronics Engineering
School of Graduate and Postdoctoral Studies
The Faculty of Engineering and Applied Science
Ontario Tech University
Oshawa, Ontario, Canada

August 2022

THESIS EXAMINATION INFORMATION

Submitted By: **MD ASHIKUR RAHMAN**

Master of Applied Science in Mechanical Engineering

Thesis title: Li-ion Battery Electrode State of Charge and Degradation Monitoring Using Battery Casing as the Reference Electrode.

An oral defense of this thesis took place on August 11, 2022, in front of the following examining committee:

Examining Committee:

Chair of Examining Committee	Dr. Martin Agelin-Chaab
Research Supervisor	Dr. Xianke Lin
Examining Committee Member	Dr. Jaho Seo
Thesis Examiner	Dr. Amirkianoosh Kiani

The above committee determined that the thesis is acceptable in form and content and that a satisfactory knowledge of the field covered by the thesis was demonstrated by the candidate during an oral examination. A signed copy of the Certificate of Approval is available from the School of Graduate and Postdoctoral Studies.

ABSTRACT

Lithium-ion battery (LIB) internal state such as state of charge (SOC), electrode capacity, and available lithium-ion monitoring is helpful for effective battery degradation monitoring. Monitoring these internal parameters is challenging due to the weak observability of the electrode parameters and lack of information about available lithium-ion contents in the cell. A reference electrode can be useful to measure the electrode potentials, which can provide information about the internal states, SOC, electrode capacity, and the available lithium-ions in the cell. In this thesis, we proposed a novel three-electrode battery setup approach using battery casing for electrode parameter estimation and degradation monitoring. The presented work introduces a curve matching algorithm to estimate electrode capacity, SOC, and available lithium-ion in the cell and an unknown input observer to estimate anode SOC and capacity. Further, electrode and cell degradation are analyzed by comparing the capacity. The proposed reference electrode setup has less impact on cell degradation compared to the existing reference electrode setup methods. In contrast, the proposed method is practically feasible regarding the practical application of three-electrode batteries for electrode level parameter estimation and available lithium-ion monitoring in the cell.

Keywords: T**hree-electrode battery, degradation analysis, electrode SOC estimation, electrode capacity, Unknown input Observer**

AUTHOR'S DECLARATION

I hereby declare that this thesis consists of original work which I have authored. This is a true copy of the thesis, including any required final revisions, as accepted by my examiners.

I authorize the University of Ontario Institute of Technology to lend this thesis to other institutions or individuals for the purpose of scholarly research. I further authorize University of Ontario Institute of Technology to reproduce this thesis by photocopying or by other means, in total or in part, at the request of other institutions or individuals for the purpose of scholarly research. I understand that my thesis will be made electronically available to the public.

MD ASHIKUR RAHMAN

STATEMENT OF CONTRIBUTIONS

Parts of this thesis have been published or submitted for publication in the following:

A. Rahman, X. Lin, "Li-ion battery individual electrode state of charge and degradation monitoring using battery casing through auto curve matching for standard CCCV charging profile", *Applied Energy, Volume 321, 1 September 2022*, doi: 10.1016/j.apenergy.2022.119367 [1]

A. Rahman, X. Lin, C. Wang, "Li-ion battery electrode state of charge estimation and degradation monitoring using battery casing via unknown input observer", *Energies 2022, 15, 5662.* doi: 10.3390/en15155662 [2]

A. Rahman, X. Lin, "Li-ion battery anode potential monitoring and charging optimization using battery casing as reference electrode", *International Green Energy Conference*, 2022

ACKNOWLEDGEMENTS

I would like to thank my supervisor, Dr. Xianke Lin, for the continuous guidance and for funding the research. His skilled guidance helped to reach my goal and develop my skills further.

I would also like to express my gratitude to the Natural Science and Engineering Research Council of Canada (NSERC) for the research fund and for creating this research opportunity.

TABLE OF CONTENTS

THESIS EXAMINATION INFORMATION ii

ABSTRACT iii

AUTHOR'S DECLARATION iv

STATEMENT OF CONTRIBUTIONS v

ACKNOWLEDGEMENTS vi

TABLE OF CONTENTS vii

LIST OF TABLES xi

LIST OF FIGURES xii

LIST OF ABBREVIATIONS AND SYMBOLS xv

Chapter 1. Introduction 1

1.1. Background and Motivation 1

1.1.1 State of Charge (SOC) and Battery Degradation 1

1.1.2 Water Glass Analogy of Lithium-ion battery 5

1.1.3 Three-electrode Cell 7

1.2. Objectives 8

1.3. Contributions 9

1.4. Outline 10

Chapter 2. Literature Review 11

2.1. Introduction 11
2.2. Battery SOC and SOH Estimation 11
2.3. Electrode Level SOC and SOH Estimation Methods 16
2.4. Three-electrode Battery Setup Methods 18
2.5. Chapter Summary 18
Chapter 3. Electrode SOC and degradation monitoring via auto curve matching 19
3.1. Introduction 19
3.2. Experimental Setup and Procedure 19
3.3. Uncertainty Analysis 23
3.4. Data Processing and Curve Matching 24
3.5. Electrode SOC, Capacity, and Remaining Cyclable Lithium Inventory Calculation 28
3.6. Chapter Summary 30
Chapter 4. Anode SOC estimation and degradation monitoring via unknown input observer 31
4.1. Introduction 31
4.2. Experimental Setup 31
4.3. Floating Anode Potential 33
4.4. Observer Design 34
4.5. Thevenin Equivalent Circuit Model 38
4.6. Model Parameter Identification 39

4.7. Anode SOC and Capacity Estimation 40
4.8. Chapter Summary 43
Chapter 5. Results 44
5.1. Introduction 44
5.2. Curve Matching Results 44
5.2.1. Cell Capacity Fade 45
5.2.2. Anode Capacity Fade and Anode SOC 46
5.2.3. Cathode Capacity Fade and Cathode SOC 48
5.2.4. Degradation Discussion 50
5.2.5. Comparison with Other Approaches 52
5.3. Unknown Input Observer Results 53
5.3.1. Cell Capacity Fade 53
5.3.2. 3-electrode Cell vs. Fresh Cell Capacity Fade 55
5.3.3. Anode Capacity Fade and Anode SOC 56
5.3.4. Degradation Discussion 58
5.3.5. Comparison to the Existing Research 59
5.4. Chapter Summary 61
Chapter 6. Conclusion and Future Work 63
6.1. Conclusion 63

6.2. Recommendations for Future Work 64

References 65

LIST OF TABLES

CHAPTER 3

TABLE I. Specifications of the tested battery 19

CHAPTER 4

TABLE II. Parameter identification results of the utilized model..... 40

CHAPTER 5

TABLE III. Capacity fade comparison..... 46

TABLE IV. Main differences in SOC and degradation monitoring techniques..... 52

TABLE V. Capacity comparison to the existing works..... 60

LIST OF FIGURES

CHAPTER 1

Figure 1.1. Lithium-ion battery degradation mechanisms. Reproduced from [3] with the permission of Elsevier. Copyright 2019 3

Figure 1.2. Most common degradation mechanisms and its effect. 5

Figure 1.3. (a) Water glass analogy: glass shrinkage due to electrode storage capacity fade. (b) Water glass analogy: water loss due to side reaction such as SEI growth and lithium plating. Reused from [1]. Copyright Elsevier 2022 6

Figure 1.4. A typical three electrode cell 7

CHAPTER 3

Figure 3.1. 3-electrode cell preparation for experiment. Reused from [1]. Copyright Elsevier 2022 21

Figure 3.2. Experiment setup. Reused from [1]. Copyright Elsevier 2022 22

Figure 3.3. Cell with rubber spacer. Reused from [1]. Copyright Elsevier 2022 22

Figure 3.4. (a) Li_xC_6 vs Al-casing Voltage [V] over cycles, (b) ideal anode voltage without shifting over cycle. Reused from [1]. Copyright Elsevier 2022 24

Figure 3.5. Voltage behavior of the cell (light green line left y-axis), Anode (blue line right y-axis) and Cathode (red line left y-axis) with respect to the reference electrode vs time (h). Reused from [1]. Copyright Elsevier 2022 25

Figure 3.6. Flowchart of the curve matching algorithm. Reused from [1]. Copyright Elsevier 2022 26

Figure 3.7. Anode curve matching over iterations. (a to d). Reused from [1]. Copyright Elsevier 2022 27

Figure 3.8. Start and end points of state of lithiation of a charging cycle. Reused from [1]. Copyright Elsevier 2022 29

CHAPTER 4

Figure 4.1. Experimental setup of three-electrode battery pack 32

Figure 4.2. $LixC6$ vs Al-casing voltage 33

Figure 4.3. Structure of the unknown input observer 35

Figure 4.4. Thevenin equivalent battery half-cell model 39

CHAPTER 5

Figure 5.1. Experimental results for cell over a CCCV charge profile: current profile, measured cell voltage, capacity. Reused from [1]. Copyright Elsevier 2022 45

Figure 5.2. Calculated anode capacity over charging cycles. Reused from [1]. Copyright Elsevier 2022 47

Figure 5.3. Anode stoichiometric range. Reused from [1]. Copyright Elsevier 2022 47

Figure 5.4. Change in stoichiometric range over charging cycles. Reused from [1]. Copyright Elsevier 2022 48

Figure 5.5. Calculated cathode capacity over charging cycles. Reused from [1]. Copyright Elsevier 2022 49

Figure 5.6. Cathode stoichiometric range. Reused from [1]. Copyright Elsevier 2022 49

Figure 5.7. Change in stoichiometric range over charging cycles. Reused from [1]. Copyright Elsevier 2022 50

Figure 5.8. Comparison between anode (blue), cathode (red) and cell capacity (light green) . Reused from [1]. Copyright Elsevier 2022 51

Figure 5.9. Experimental results of the battery pack over a CCCV charge profile: current profile, measured voltage 53

Figure 5.10. Experimental results of an individual cell in the battery pack over a variable current charge profile: current profile, measured cell voltage, capacity 54

Figure 5.11. Comparison between fresh cell and 3-electrode cell capacity fade 55

Figure 5.12. Anode capacity graph over cycles 56

Figure 5.13. Estimated anode SOC or stoichiometric range 57

Figure 5.14. Comparison between anode (blue) and cell capacity (light green) 59

Figure 5.15. Comparison between estimated anode SOC and the reference anode SOC form for standard CCCV charging profile for a single three-electrode cell 60

Figure 5.16. Comparison between estimated anode capacity and the reference anode capacity form for standard CCCV charging profile for a single three-electrode cell 61

LIST OF ABBREVIATIONS AND SYMBOLS

Ah	Ampere-hour	**UIO**	Unknown Input Observer
BMS	Battery Management System	**LMI**	Linear Matrix Inequalities
BP	Back-Propagation	**GPR**	Gaussian Process Regression
CC	Constant Current	**LSM**	Least-Squares Method
CV	Constant Voltage	**ANN**	Artificial Neural Network
EV	Electric Vehicles	**SGP**	Standard Graphite Potential
FFNN	Feedforward Neural Network		
LFP	Lithium Iron Phosphate		
LAM	Loss of Active Material		
LLI	Loss of Lithium Inventory		
LMO	Lithium-ion Manganese Oxide		
LTO	Lithium Titanium Oxide		
NMC	Nickel Manganese Cobalt Oxide		
NN	Neural Network		
OCV	Open-Circuit Voltage		
RC	Resistor-Capacitor		
SEI	Solid Electrolyte Interface		
SOH	State of Health		
SOC	State of Charge		
SOL	State of Lithiation		

Chapter 1. Introduction

1.1. Background and Motivation

Lithium-ion batteries are now the most popular energy storage device for the automotive industry. LIBs are in high demand as an energy storage medium, mainly due to their high energy density, long service life, slow self-discharge rate, and zero harmful gas emission. Especially the increasing demand for lithium-ion batteries in electric vehicles (EVs) made researchers interested in improving battery technology further to enhance its performance and reliability. This development vastly depends on the battery's internal state information, such as the state of charge, degradation patterns, and degradation status of the electrodes. Accurate estimation or calculation of these states in real-time will help prolong the battery service life through optimal charging conditions and also enable us to analyze the reusability of the EV battery when it retires from service upon reaching an 80% state of health. Model-based estimation techniques are complex and not always easy to employ in the battery management system. A reference electrode can help measure electrode potentials, providing electrode level states for better monitoring. Most existing reference electrode setup methods are feasible for research purposes only. Moreover, the safety risk is also associated with such 3-electrode setup methods.

1.1.1 State of Charge (SOC) and Battery Degradation

Lithium-ion batteries (LIB) are the most commonly used energy storage device in electric vehicles (EVs) and stationary energy storage systems due to their low self-discharge rate, long service life, and, more importantly, high energy density. However, lithium-ion battery performance is greatly affected with time and usage over LIB service

life by the side reactions in the battery during operation. Therefore, it is critical to understand the internal status, for instance, state of charge, lithium inventory, and degradation status over cycling, and monitor it throughout the service life to ensure battery safety and performance.

The degradation of lithium-ion batteries is an irreversible and complex phenomenon and an essential parameter to monitor in the BMS. These degradation mechanisms are mainly a result of various side reactions, including chemical and mechanical reactions [3]. These reactions result in battery capacity loss per full charge and fail to meet the power output requirements due to the increased internal resistance. Cell capacity and internal resistance are among the most used parameters to quantify lithium-ion battery degradation. Capacity is the total amount of charge a battery can store during a charging cycle. At the same time, internal resistance is the parameter to measure how quickly a cell can output the stored energy. A degraded cell has less energy storage capacity caused by various degradation mechanisms. The internal resistance increase affects the battery performance by providing less energy output for the same withdrawing current compared to the fresh cell. The battery state of charge is calculated by dividing the capacity at any state by the nominal capacity. This thesis presents state and parameter estimation for a single cell and an individual cell in a battery pack; thus, it mainly focuses on a single cell parameter estimation.

The most conventional way of determining SOC is by monitoring capacity fade [4]. Over cycling, the capacity of the lithium-ion battery decreases caused of various side reactions. A fully charged degraded cell will output less energy compared to the fresh cell. The amount of charge it can output is significant for electric vehicle applications; thus, the

state of charge is calculated based on the capacity at any state to the fresh cell capacity given by the equation (1.1).

The most common form of SOC calculation is as follows [5],

$$SOC(t) = SOC_0 + \frac{1}{Q_n}\int_{t_0}^{t} I(t)dt \tag{1.1}$$

where SOC_0 is the initial SOC, Q_n is the nominal cell capacity, $I(t)$ is the applied current to the battery during charge or discharge.

Various irreversible degradation mechanisms cause the capacity fade in lithium-ion batteries. The degradation mechanisms result from various side reactions in electrodes, electrolytes, and current collectors. Fig. 1.1 shows some of the most common Li-ion battery degradation mechanisms.

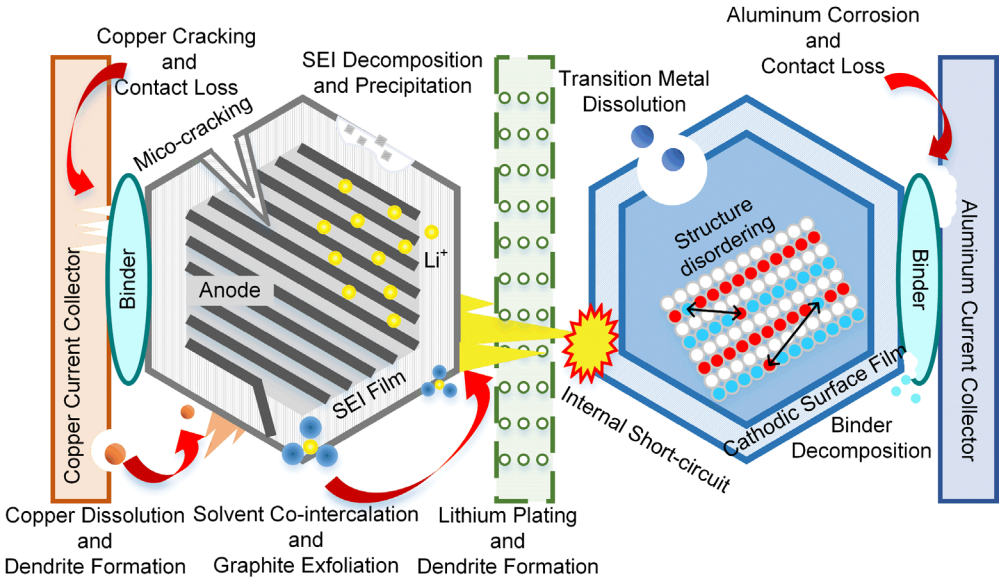

Figure 1.1. Lithium-ion battery degradation mechanisms. Reproduced from [3] with the permission of Elsevier. Copyright 2019

These degradation mechanisms result in overall capacity fade through cyclable lithium-ion loss, loss of active electrode material, internal resistance increase due to SEI formation, and current collectors contact loss. Identifying the specific mechanism responsible for the capacity fade is very challenging. Thus, similar kinds of degradation mechanisms can be grouped for better degradation understanding, as recommended by [6] and [7].

Degradation mechanisms can be grouped as follows [8]:

Loss of lithium inventory (LLI): The consumption of lithium-ions through side reactions results in a loss of lithium inventory (LLI) [9]. The most significant side reactions that cause LLI can be listed as solid electrolyte interface (SEI) formation on the electrode surface, electrolyte decomposition, and lithium plating. SEI is a passivation layer [10] on the electrode formed by electrolyte decomposition, as shown in Fig. 1.1. The SEI growth consumes the cyclable lithium ions and electrolytes, resulting in LLI [11], [12]. Unfavorable LIB operating conditions such as fast charging or low-temperature charging could cause another significant anode side reaction called lithium plating[13], [14]. The metallic lithium formation around the anode of LIBs during charging is known as lithium plating [3], [15].

Loss of active material (LAM): LAM can be caused by the transition metal dissolution and structure disordering [3], graphite exfoliation [16], binder decomposition [3], electrode particle cracking[10], [3], and current collectors' electrical connection loss [3]. The transition metal dissolution of cathode material could occur at high charging voltage [16], and the dissolved metal can deposit on the anode[3], [16], [17].

Most of the above-discussed degradation mechanisms either contribute to loss of lithium inventory or loss of active material (LAM), which collectively causes capacity fade. This thesis focuses on the outcomes of various degradation mechanisms through monitoring the lithium-ion inventory and the electrode storage capacity degradation, reflecting the LLI and LAM, respectively.

Fig. 1.2 [18] demonstrates the most common degradation mechanisms and their effect on lithium-ion batteries.

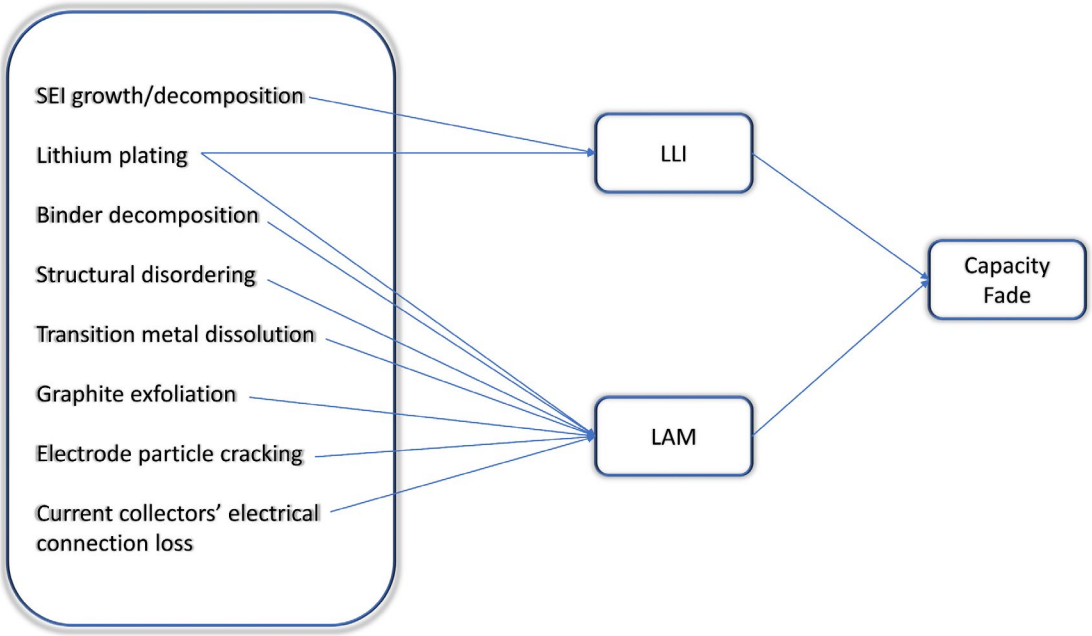

Figure 1.2. Most common degradation mechanisms and its effect.

1.1.2 Water Glass Analogy of Lithium-ion battery

The side reactions affect the LIB performance in different ways. Some cause cyclable lithium loss and others result in storage capacity fade of each electrode. The water-glass analogy can explain this complex degradation mechanism. The electrodes are

considered two glasses that carry lithium ions like water and exchange the water during charge and discharge cycles. The storage capacity fade of the electrodes caused by various side reactions described above is represented by the volume shrinkage of the glasses, and the water loss represents cyclable lithium loss. As the capacity of electrodes fades away

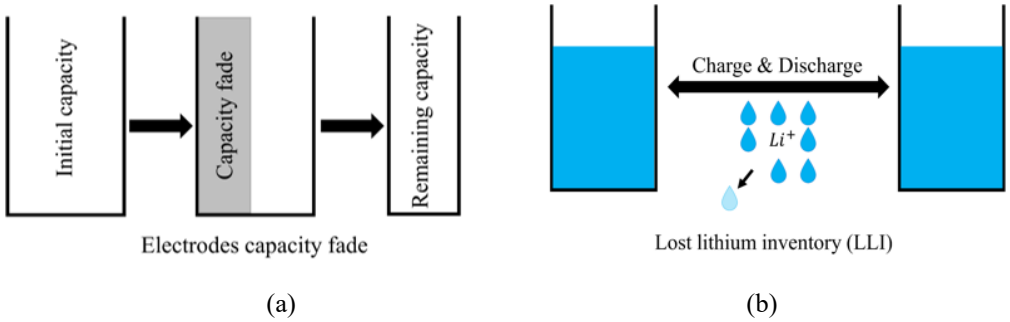

(a) (b)

Figure 1.3. (a) Water glass analogy: glass shrinkage due to electrode storage capacity fade. (b) Water glass analogy: water loss due to side reaction such as SEI growth and lithium plating. Reused from [1]. Copyright Elsevier 2022

due to various side reactions, such as graphite exfoliation, transition metal dissolution, structure disordering, and electrode particle cracking over a long cycling period, as shown in Fig. 1.3(a), the glass, which represents the electrode, will shrink and be filled up faster. Lithium ions (water) are transported between the electrodes (glasses) through the separator during charge and discharge, and some of these lithium ions (water) get lost through SEI and lithium plating during the cycling process shown in Fig. 1.3(b). Both the electrode storage capacity loss (glass volume shrinkage) and cyclable lithium loss (water loss) contribute to the overall battery degradation [6], [9], [16], [20], [21]. Therefore, monitoring both electrodes' capacity fade and the cyclable lithium inventory in the LIB is crucial.

1.1.3 Three-electrode Cell

Typically, a Li-ion battery has two electrodes, the positive and negative electrodes, widely known as cathode and anode. To understand degradation in the electrodes, the electrode potential data is essential. The electrode potential can only be measured with respect to a reference material or a third electrode in the cell known as the reference electrode. A third or reference electrode is required to study the individual electrode potential. The voltage measurement of each electrode with respect to a reference electrode gives us the potential of that electrode [19]. Various factors are considered when selecting a reference electrode, such as the equilibrium potential of the reference electrode material, impact on the electrolyte and electrode materials, and impact on the battery design and fabrication [20]. Lithium metal is most commonly used as a reference electrode in lithium-ion batteries [21]–[24]. However, lithium metal is mainly used in the lab for material

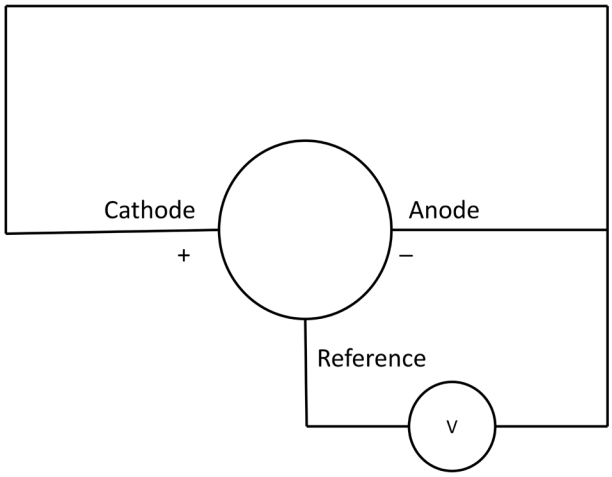

Figure 1.4. A typical three electrode cell

research, not suitable for practical applications. Because Li is a very reactive material that can continuously react with electrolytes and consume the electrolyte in the battery [25] and also inserting a metal lithium reference electrode inside the battery could short-circuit the

battery. Other materials that are used as reference electrodes include Li-Al, Li-Sn, Li-Au alloys, and lithium iron phosphate (LFP), lithium titanium oxide (LTO) [20]. Fig. 1.4 illustrates a typical 3-electrode battery.

1.2. Objectives

The main goal of this research is to contribute towards the degradation monitoring of lithium-ion battery single cell and individual cells in a battery pack and introduce an innovative electrode level degradation monitoring method with fewer sensors and external equipment.

The detailed objectives of this research include:

1. Developing a three-electrode battery setup method using the battery casing as a reference electrode.
2. Developing a method to calculate individual electrode state of charge and capacity along with lithium inventory monitoring.
3. Setting up a three-electrode battery pack for individual battery anode parameter estimation.
4. Developing a mathematical model-based anode SOC and capacity estimation method using Thevenin equivalent circuit model.

1.3. Contributions

To the best of the author's knowledge, the main contributions of this research are listed below:

1. The battery casing is proposed as the reference electrode for electrode potential measurement. This novel approach enables calculating and monitoring of the status of electrodes and cyclable lithium, which are valuable to the BMS to further optimize the operating parameters.
2. A curve matching algorithm is proposed to solve the electrode floating voltage issue while measuring electrode voltages with respect to the reference electrode. The developed algorithm is also able to monitor the lithium-ion inventory in real-time
3. The electrode's state of charge and capacity fade calculation and monitoring method is proposed.
4. A three-electrode battery pack setup is proposed using a battery casing as the reference electrode. Using casing as a reference for the three-electrode battery pack is beneficial for estimating individual battery electrode parameters, such as electrode capacity fade and state of charge.
5. A model-based anode state of charge estimation method is developed using an unknown input observer for an individual battery in the battery pack.
6. The anode state of the charge estimation method for variable charge and discharge current is developed.
7. A capacity fade estimation method of the anode of an individual cell in the battery pack is proposed.

1.4. Outline

This thesis is organized as follows:

- **Chapter 1** presents the background and motivation of this research along with its contributions.
- **Chapter 2** will review the existing literature on the related field and its current methodologies.
- **Chapter 3** will present the concepts and the developed methodologies for electrodes SOC and degradation monitoring.
- **Chapter 4** will describe the developed methodology for the anode SOC estimation and degradation monitoring.
- **Chapter 5** will present the results and a detailed discussion of this research.
- **Chapter 6** will conclude this thesis and suggests future work on the presented topics.

Chapter 2. Literature Review

2.1. Introduction

This chapter will review various SOC/SOH estimation methods for lithium-ion batteries. There is a lack of studies on electrode level SOC estimation. However, some recent electrode level SOC estimation methods are also reviewed in this chapter. Then, various three-electrode lithium-ion battery setup method is illustrated.

2.2. Battery SOC and SOH Estimation

Among the most critical battery internal parameters, the energy indicating parameter state of charge (SOC) provides remaining capacity information in the battery. Accurate SOC estimation in the battery management system is critical for reliability and for prolonging battery life. Various SOC estimating methods have been developed considering different approaches [26]–[28], [29]. Ampere-hour (Ah) or coulomb counting estimating method [26], [27], [30]–[32]is the most conventional among the estimation methods used based on calculating transferred charge to the cell by integrating charge and discharge current over time. This low-cost computational method can estimate SOC in real-time. However, the significant drawbacks of this technique are measurement error accumulation during operation [30], [33]and it requires a known initial SOC in the algorithm. The open-circuit voltage (OCV) measurement method [26], [32], [34], [30], [35] is another widely used SOC estimation technique. However, it is very time-consuming due to its long resting time requirement for voltage stabilization [30] and not very practical for real-time battery management applications as it is almost impossible to measure the OCV voltage during battery operation. The accurate SOC estimation using the OCV method

heavily depends on the OCV-SOC relationship [36], [37]. There are many studies on model-based methods which calculate SOC using an equivalent circuit model or a simplified physics-based model [28], [38], [39], [40]. However, these models face weak observability issues, especially for the batteries with flat cathode potential [41]. Neural network-based methods have been gaining traction in recent years. They are useful for SOC estimation due to their nonlinear mapping capability [30], [35], [42]. However, the complexity of neural networks and high computational cost are significant drawbacks. It also requires a considerable amount of training data under various conditions. Mathematical model-based estimation techniques[28], [38], [39], [41] gained popularity in EV applications due to their estimation reliability while employed in EV real-time applications. These methods are developed using a battery model with a mathematical model to estimate SOC [39], [43], [44], [45]. The performance and reliability of this method can be further improved by employing an observer or adaptive filters [26].

There have been numerous methodologies developed for SOC and state of health (SOH) estimation based on different estimation techniques such as adaptive filter, machine learning, or observer-based [26], [32], [46]. Many SOC and state of health (SOH) estimation methods have been proposed based on electrochemical [47], [48] and electrothermal [30], [35], [49] models. J. Li *et al.* [17] developed a single particle degradation model that considers only SEI layer formation to estimate the SOH of the LIB. This SOH estimation method is based on a simplified degradation model, which may not reflect the actual degradation in the battery. Y. Ma *et al.* [38] proposed a SOC estimation method of LIB based on the fractional-order impedance spectra model. In this approach, the battery fractional order impedance model is first derived. The model parameters for the

LIB are identified using a frequency fitting method and parameter identification algorithm. A Kalman filter approach is then introduced to estimate the SOC. This approach involves many models and complex calculations to estimate the SOC. D. Andre *et al.* [39] presented two SOC and SOH estimation methods using the Kalman filter and unscented Kalman filter coupled with a support vector regression algorithm. The estimation accuracy of the model is verified by experimental data [50], [51]. Lai *et al.* [52] developed an equivalent circuit model considering partial electrochemical properties. Battery parameters are then identified using a particle swarm optimization method. Then an extended Kalman filter is employed to estimate SOC. They have achieved less than 1% estimation error for the proposed estimation method. The proposed method adopted multiple algorithms to develop the estimator, thus introducing application complexity. Dai *et al.* [53] proposed an online cell SOC estimation method in a battery pack. An equivalent circuit model is developed for the battery, then the battery pack's average SOC is estimated. Then the performance divergences between the "averaged cell" and each cell are incorporated to estimate SOC for all cells using an extended Kalman filter. Y. Zou *et al.* [54] developed a combined SOC and SOH estimation method using the Kalman filter. First, the SOC dependency of the common parameters of a first-order RC (resistor-capacitor) model is determined. Then, the performance degradation of the model is quantified. Last, two Kalman filters of different time scales are employed to estimate SOC/SOH. He *et al.* [55] developed a cell SOC estimation method based on an adaptive Kalman filter. They have proposed an improved Thevenin battery model by adding an additional RC branch. The battery model parameters are identified using an extended Kalman filter algorithm. Then, an adaptive Kalman filter algorithm is employed to estimate the SOC of the lithium-ion battery. The proposed

method improves the estimation by reducing the maximum SOC estimation error from 14.96% to 2.54% and 3.19% to 1.06% for the mean SOC estimation error. X. Tang *et al.* [41] presented a multi-gain observer-based SOC estimation method. A classifier was used to select the gain for the observer to increase the convergence speed. The accuracy of this estimation method depends heavily on the observer. Snoussi *et al*. [56] proposed a cell SOC estimation method based on an unknown input observer and a differential-algebraic model. The proposed observer uses initial SOC as an unknown value for the system. First, open circuit voltage is estimated using a reduced-order unknown input observer and then the SOC is estimated using the OCV-SOC characteristic offline-determined. Rao *et al.* [57] proposed a nonlinear fractional-order unknown input observer (FOUIO) based cell SOC estimation method. They have utilized linear matrix inequality-based formulation for the parameter matrices calculation. The proposed method was then validated and compared with reported SOC estimation methods. Xu *et al.* [58] developed a proportional-integral (PI) observer-based lithium-ion battery SOC estimation method. They have utilized a simple-structure RC battery model to model the Li-ion battery. They achieved estimation error within 2% for both the known and unknown initial SOC. Zhong *et al.* [59] proposed an adaptive sliding mode observer (SMO) based SOC estimation. A fractional order equivalent circuit model (FOECM) is utilized to model the lithium-ion battery. To reduce chattering and convergence time they have presented a new self-adjusting strategy for the observer gains that adjusts the observer in the estimation process. Guo *et al.* [60] presented an improved BP neural network-based SOC estimation algorithm. This method achieved a better result by significantly reducing the SOC prediction error by utilizing a lot of experimental data to improve NN training and learning. Guo *et al.* [61] proposed a SOH

estimation method employing an equivalent circuit model to characterize the CC part of the charging curve and derived a transformation function and a time-based parameter. Equivalent circuit model parameters are evaluated using a nonlinear least-squares method (LSM). A. Mohamed *et al.* [62] presented a SOC estimation technique using an adaptive neuro-fuzzy inference system. The proposed method estimates SOC using the OCV and SOC relationship information provided by the cell manufacturer. OCV-based SOC estimations are time-consuming and not suitable for real-time estimation applications due to the difficulty of measuring OCV during operation. Chen *et al.* [63] proposed a state of charge estimation method based on an inclusive equivalent circuit model. Battery model parameters are estimated using a neural network. A nonlinear observer is designed based on a radial basis function neural network to estimate the battery's SOC. The proposed method has a faster convergence speed and higher precision compared to the Kalman filter-based SOC estimation algorithms. Chen *et al*. [64] developed a neural network and Kalman filter-based battery SOC estimation method. They presented an improved battery model based on a feedforward neural network (FFNN). A SOC estimating algorithm is then developed based on an extended Kalman filter. The robustness of the developed model and algorithm is then verified using a hardware-in-loop test bench. He *et al.* [65] proposed an artificial neural network (ANN)–based SOC estimation method. An ANN is utilized to develop a battery model for SOC estimation with an unscented Kalman filter to reduce estimation error. Dang *et al.* [66] presented an OCV-based SOC estimation method using a dual neural network. The battery is modeled using two neural networks connected in series. A linear neural network is employed to identify first-order or second-order electrochemical model parameters. Then, a BP neural network is used to capture the OCV-

SOC relationship. An average estimation error of 1.03% is achieved with a maximum error of 4.82%. Boujoudar *et al.* [67] presented a SOC estimation method based on FFNN and the nonlinear autoregressive (NARX) model. Both neural networks are first trained offline and then employed to estimate SOC (NARX is used to estimate the SOC, and FFNN is used to identify battery parameters). Wei *et al.* [68] employed an improved dynamic neural network to estimate the SOC through an open-loop and a closed-loop nonlinear auto-regressive model. This method utilized multiple models and a dynamic NN which introduces more complexity. He *et al.* [69] propose an artificial neural network–based lithium-ion battery model for SOC estimation, based on the measured current and voltage. In the proposed method SOC estimation error is reduced by employing an unscented Kalman filter. Then the method is validated using LiFePO4 battery data. To reduce the complexity of employing model-based SOC estimation methods for battery packs, Deng *et al.* [70] proposed a data-driven SOC estimation method for battery packs based on gaussian process regression (GPR). First, features are extracted through correlation analysis and principal component analysis to obtain an input dataset with a high correlation with SOC. Second, the wights of the features are optimized by utilizing the squared exponential kernel function and automatic relevance determination. To improve the estimation accuracy, the authors used an autoregressive GPR model along with the regular GPR model. The estimation error achieved in this study is lower than 3.9%.

2.3. Electrode Level SOC and SOH Estimation Methods

The existing SOC and SOH estimation methods are mostly model-based and do not directly measure the battery's internal parameters except voltage and current. They are heavily dependent on the degradation information from the model [16], [71], [72], which

may not reflect the degradation in the actual battery cells due to the degradation complexity and low model fidelity. The neural network (NN) based SOC estimation models[73] are trendy these days, but the drawback of NN-based methods is the large amount of data required to train the network for better accuracy. These methods' computational cost and implementation complexity are also troublesome for real-time applications. One key issue is that most studies in this field focus on the cell level SOC and SOH and cannot provide the status information at the electrode level inside the battery.

S. Lee *et al.*[74] proposed two model-based methods (voltage fitting and differential voltage analysis) to estimate the electrode state of health of NMC/graphite cells using half-cell potential. The proposed method can separate individual electrodes' voltage contribution from the cell voltage by utilizing peak information in the differential voltage curve. A. Bartlett *et al.*[40] proposed an electrochemical model to estimate the SOC and capacity of a lithium-ion manganese oxide (LMO)-NMC composite electrode Li-ion battery. Their study presents a reduced-order electrochemical model to predict the electrode's surface and bulk lithium concentration. Tian *et al.* [10] presented an electrode level parameter estimation method via a convolutional neural network. The proposed method can estimate electrode capacities and initial SOCs from the parts of the charging profile without feature extraction, which enables electrode fast aging diagnosis. Further, these estimated parameters are used to reconstruct OCV-Q (charge amount) curves that can estimate battery capacity with an accuracy of more than 99%. These electrode SOC/SOH estimation methods are model-based, and the used electrochemical models do not degrade over time. Therefore, the estimation algorithms face issues when the battery experiences considerable degradation over cycling.

2.4. Three-electrode Battery Setup Methods

McTurk *et al.* [75] presented an approach to insert a Li metal foil or Li-plated copper rod as a reference electrode in a commercially available pouch cell. They made a 5mm cut in the pouch cell, and then the shell was pilled to open the cell. A U-shaped lithium metal foil is used as the reference electrode. D. Aurbach *et al.* [15] presented another approach by cutting a commercial cylindrical cell and forming two half cells using the electrodes of the cell. Somerville, L *et al.* [76] proposed a new approach by cutting a commercially available cylindrical cell and inserting a Li metal reference electrode. They tabbed the cell first with stainless steel tabs, then using a pipe cutter, they cut the cell between the cap and the shell. The reference electrode used for this is prepared by wrapping lithium metal around a copper wire. However, these are not promising approaches for practical applications because inserting additional reference electrode materials into the battery could cause additional side reactions, change the battery manufacturing process significantly, increase production cost, and risk internal short-circuit.

2.5. Chapter Summary

This chapter discusses various lithium-ion battery and electrode SOC/SOH estimation methodologies and popular three-electrode battery setup methods. The chapter starts by discussing Li-ion battery SOC and SOH estimation methods, followed by the electrode level SOC estimation methods. Then existing most conventional three-electrode battery setup methods are discussed.

Chapter 3. Electrode SOC and degradation monitoring via auto curve matching

3.1. Introduction

This chapter will cover the three-electrode battery setup method along with the experimental setup for the research. Followed by the data processing technique and developed curve matching algorithm. Furthermore, both electrode SOC and capacity calculation method are discussed in detail.

3.2. Experimental Setup and Procedure

Commercially available 18650-type cells (UR18650AA, Sanyo) are used in this study. The cell consists of graphite anode and lithium nickel manganese cobalt oxide (NMC) cathode. The nominal capacity and voltage of the cell are 2.25Ah and 3.6V, respectively. Before the experimental setup, the cell was discharged to its standard cut-off voltage of 2.5V. The experiment is conducted at a room temperature of 25°C. Standard cell specification is shown in Table I.

TABLE I. Specifications of the tested battery

Specification	Cell
Cell type	UR18650AA. Sanyo
Electrode material	$Li(Ni_{0.8}Co_{0.1}Mn_{0.1})O2$ / graphite
Nominal capacity	2.25Ah
Minimum capacity	2.15Ah
Charge cut-off voltage	4.2V
Nominal voltage	3.6V

Discharge cut-off voltage	2.5V
Charge and Discharge cut-off current	0.02C
Standard charging current	0.7C
Testing temperature	25 ℃

The battery casing is used as a reference electrode for this experiment. The cell was connected with nickel tabs at three locations: positive and negative terminals and the shell. The cell's casing was then cut very carefully while holding vertically to isolate it from the negative electrode. After the reference casing was cut (disconnected from the cell's negative terminal), a non-reactive silicone glue was used to seal the cut. An anode voltage of 2.7V and a cathode voltage of 0.8V with respect to the reference electrode was observed right after the cut. The prepared cell is then left to rest. At this point, we have a working cell with a negative, positive, and reference electrode.

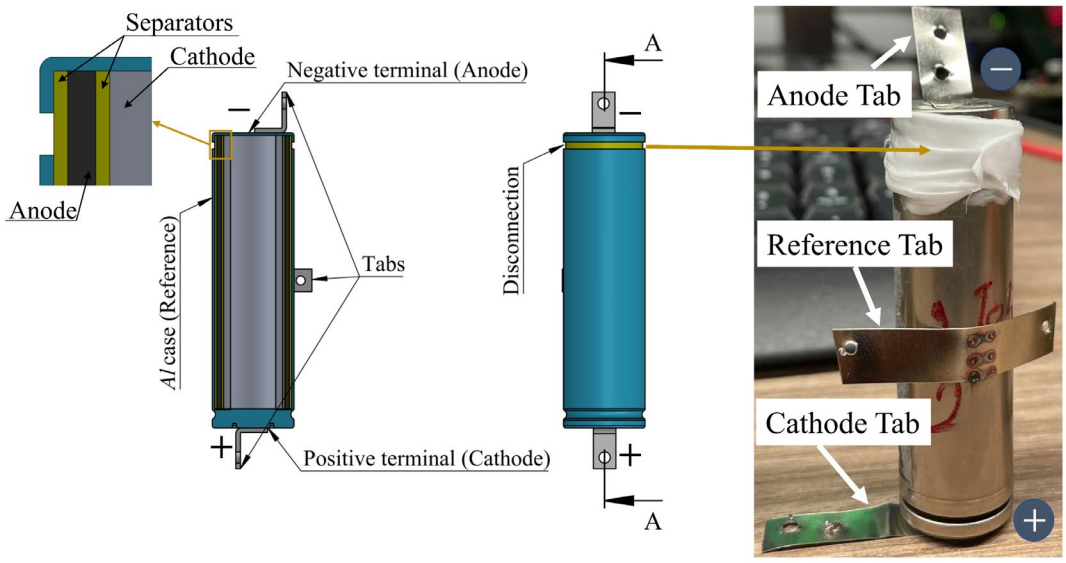

Figure 3.1. 3-electrode cell preparation for experiment. Reused from [1]. Copyright Elsevier 2022

The cell is then kept vertically overnight to dry up the silicon glue. Fig. 3.1 shows the three-electrode cell setup for the experiment. Cell negative and positive electrodes are then connected to the cable of the cycler for cycling, and the reference electrode and negative electrode are connected to another cable of the cycler to record the voltage difference between the anode and reference electrode. Cathode voltage is obtained by getting the difference between the anode potential and the full-cell voltage. The cell was then cycled using standard constant-current constant-voltage charge and discharge protocol. A standard charging current of 0.7C (1505mA) was applied for both charging and discharging, where cut-off voltages for charge and discharge were set to 4.2V and 2.5V, respectively. 1/50 C or 43mA cut-off current is used for both charging and discharging. The anode voltage (with respect to the reference electrode) is recorded during the charging and discharging cycles.

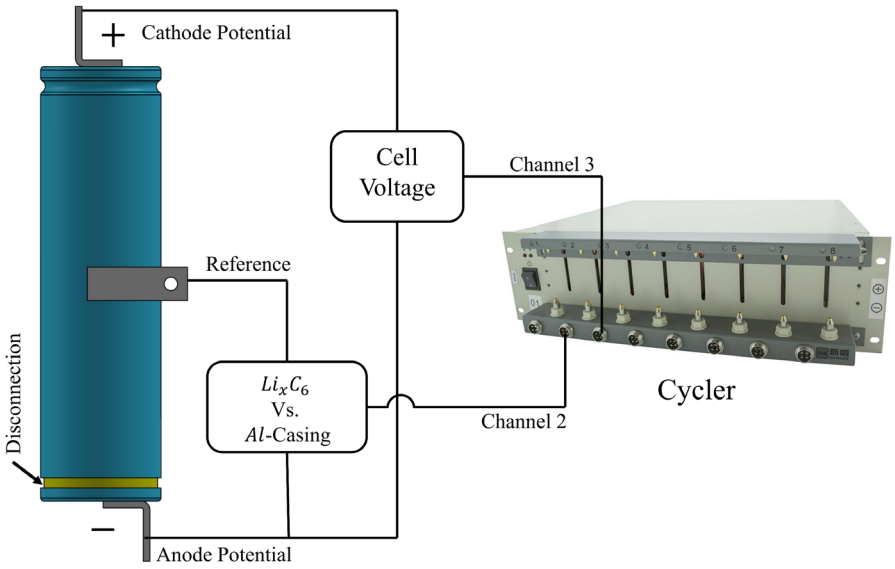

Figure 3.2. Experiment setup. Reused from [1]. Copyright Elsevier 2022

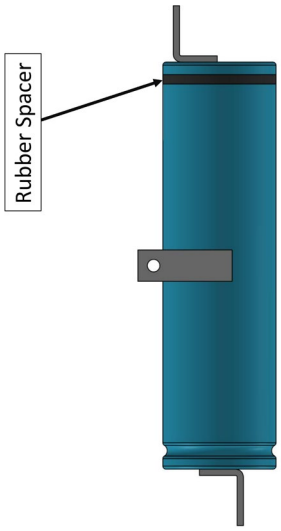

Figure 3.3. Cell with rubber spacer. Reused from [1]. Copyright Elsevier 2022

The experimental setup is shown in Fig. 3.2. To produce similar three-electrode cells in the commercial products, the casing can be manufactured using a rubber spacer between the negative terminal portion of the casing and the reference casing, as shown in Fig. 3.3. The spacer will help separate the reference casing from the negative electrode and seal the gap

to produce a three-electrode cell. This manufacturing process does not add any extra new material and is very cost-effective and safe.

3.3. Uncertainty Analysis

We observe that the measured anode voltage gradually and slowly shifts up and down over cycling. This can be described using the Nernst equation. In a redox reaction, the potential is determined by the Nernst equation [77], which is shown below,

$$E = E^0 - \frac{RT}{nF} ln\, C \tag{3.1}$$

where E, E^0 represents reduction and standard potential, respectively. R, F is gas constant and Faraday constant, T is the ambient temperature in kelvin, n is the number of electrons transferred in the reaction, and C is the reaction quotient which is the relative amounts of products and reactants available during a reaction at a particular time. As shown in Eq. 3.1, E is affected by the metal ion concentration C in the solution. Based on Eq. 3.1, the shift of electrode potential is due to the uncertainty and variation of metal-ion concentration in the solution. The voltage shift of Li_xC_6 with respect to the battery, the casing is shown in Fig. 3.4(a).

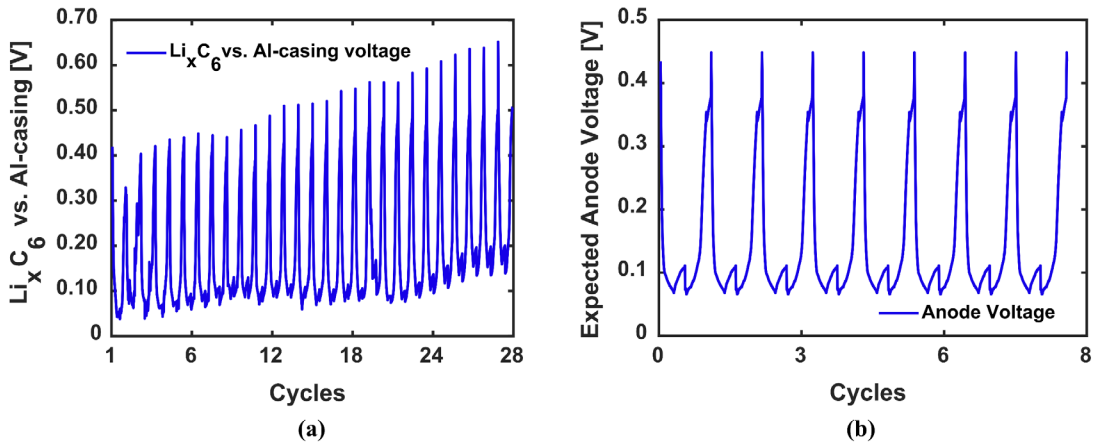

Figure 3.4. (a) Li_xC_6 vs Al-casing Voltage [V] over cycles, (b) ideal anode voltage without shifting over cycle. Reused from [1]. Copyright Elsevier 2022

As shown in Fig. 3.4(a), the measured anode voltage shifts up and down over time due to the unknown concentration of Al^{3+} change in the solution. Without this floating voltage issue, the anode voltage curve should look similar to Fig. 3.4(b). Due to the voltage floating issue, we can not use the anode potential directly to calculate the electrode SOC and storage capacity. To address this issue, we proposed a voltage curve matching approach that matches the floating curve to the standard anode curve since the shape of the anode voltage curve remains similar to the standard graphite potential. Thus, this approach is helpful in obtaining the stoichiometric information of the electrodes after each cycle.

3.4. Data Processing and Curve Matching

Recorded battery cycling data (input current and measured voltage), anode, and cathode voltage are processed using MATLAB for further calculation. Anode, cathode, and cell data were matched based on the recorded timestamp to avoid data mismatch. Fig 3.5 shows the cell voltage along with the anode and cathode voltages.

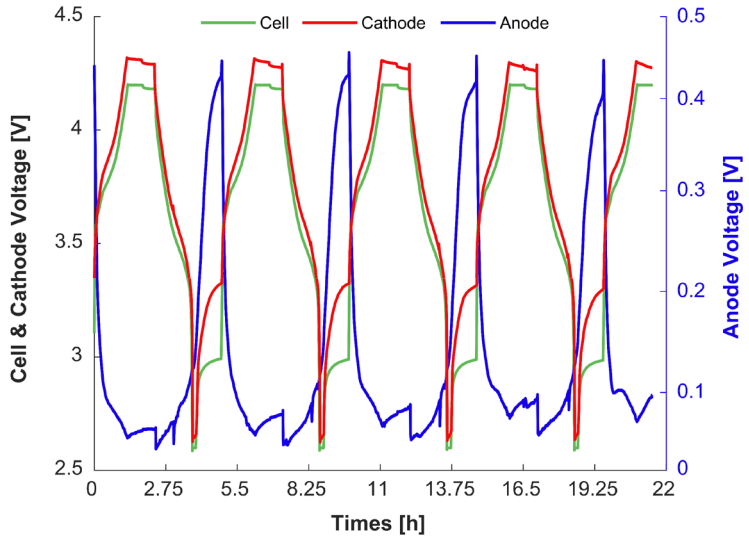

Figure 3.5. Voltage behavior of the cell (light green line left y-axis), Anode (blue line right y-axis) and Cathode (red line left y-axis) with respect to the reference electrode vs time (h). Reused from [1]. Copyright Elsevier 2022

The cell anode is made of graphite material. Therefore, the standard graphite anode potential curve is used for anode voltage curve matching, and the NMC half-cell cathode potential curve is used to match the recorded cathode voltage. Curves are matched to find the starting and endpoint of the state of lithiation (SOL) during a charging cycle. The lithiation status shows the percentage of lithium-ion transferred from anode to cathode during the charging cycle.

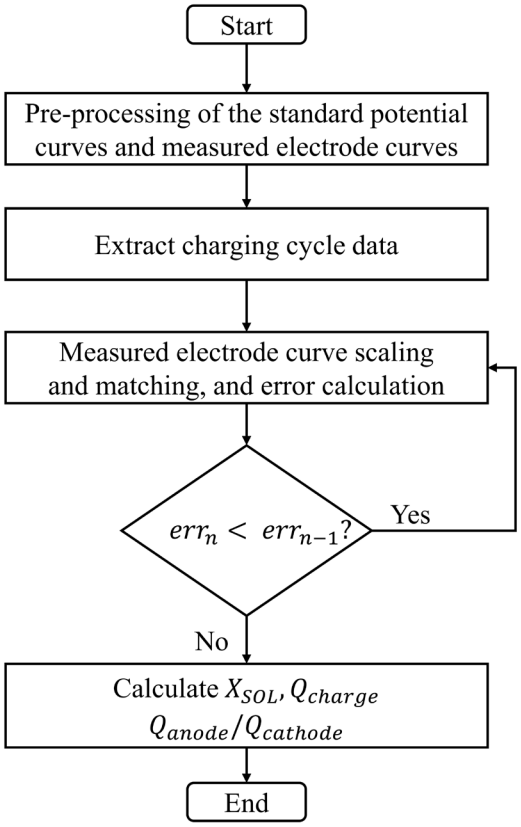

Figure 3.6. Flowchart of the curve matching algorithm. Reused from [1]. Copyright Elsevier 2022

Curves are matched based on the iterative chi-squared error reduction method [78]. The voltage curves of anode and cathode during a charging cycle are matched with the standard graphite potential and NMC cathode potential curve. Standard anode and cathode curves are fixed for the matching process, while the measured anode and cathode voltage curves are scaled to match the standard curves. The error of the curve matching is calculated using Eq. 3.2. An algorithmic flowchart of error calculation and curve matching is shown in Fig. 3.6.

$$err = \sum_i^n (R_i - E_i)^2 \tag{3.2}$$

where R_i, E_i represent the i-th values of the standard potential curve and measured electrode curve, respectively. The error of the i-th iteration is compared with the (i-1) iteration. When the error cannot be further reduced, the algorithm exits iteration.

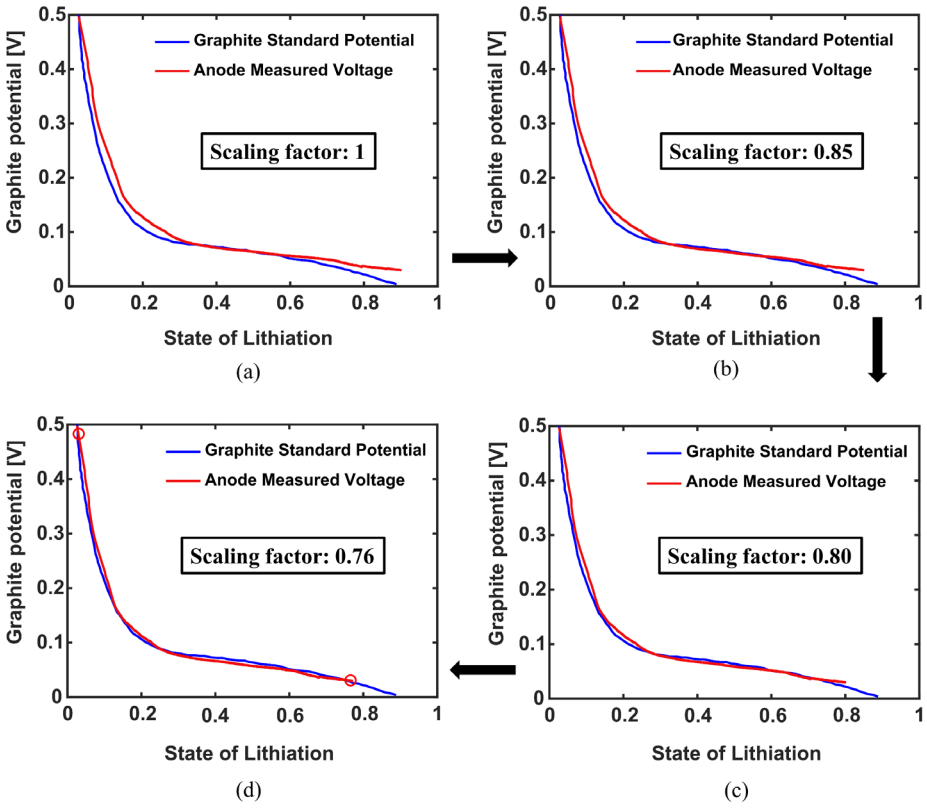

Figure 3.7. Anode curve matching over iterations. (a to d). Reused from [1]. Copyright Elsevier 2022

Fig. 3.7 (a to d) shows the curve matching over iterations. The curve's start and endpoint (shown in Fig. 3.7(d) marked in red circle) are used to calculate each electrode's SOL.

3.5. Electrode SOC, Capacity, and Remaining Cyclable Lithium Inventory Calculation

During the constant current (CC) charging stage, the charging current remains constant, thus, Q_{CC} is calculated by multiplying the current with charging time which is demonstrated in Eq. 3.3, but the current decreases over time for the constant voltage (CV) charging stage. Therefore, Q_{CV} is calculated by integrating the current over the charging time as shown in Eq. 3.4. The amount of charge transferred during a charging cycle is calculated by adding the capacity of the constant current charging part and the constant voltage charging part as shown in Eq. 3.5 below.

$$Q_{cc} = I \cdot (t_{end\_cc} - t_{0\_cc}) \tag{3.3}$$

$$Q_{cv} = \int_{t_{0\_cv}}^{t_{end\_cv}} I(t)\, dt \tag{3.4}$$

$$Q_{charge} = Q_{cc} + Q_{cv} \tag{3.5}$$

where Q_{cc} and Q_{cv} represent the amount of charge transferred during constant current and constant voltage charging stages, t_0 and t_{end} represent the starting and ending times of each stage (CC and CV). I represent the constant current of CC stage and $I(t)$ represent the CV stage current as a function of time. Q_{charge} represent total charge transferred to the cell during a charging cycle.

The start and end points are the points on the X-axis of the standard graphite potential curve that matches with the first and last point of the measured anode voltage curve. The start and end points of cathode SOL are found following the same method as the anode.

$$X_{diff} = |X_{end} - X_{start}| \tag{3.6}$$

where $X_{diff}, X_{start}, X_{end}$ represent the percentage difference in the state of lithiation after charging, state of lithiation when the charging cycle is started, and state of lithiation when the charging cycle ends, respectively. The remaining cyclable lithium in the battery is calculated using Eq. 3.6.

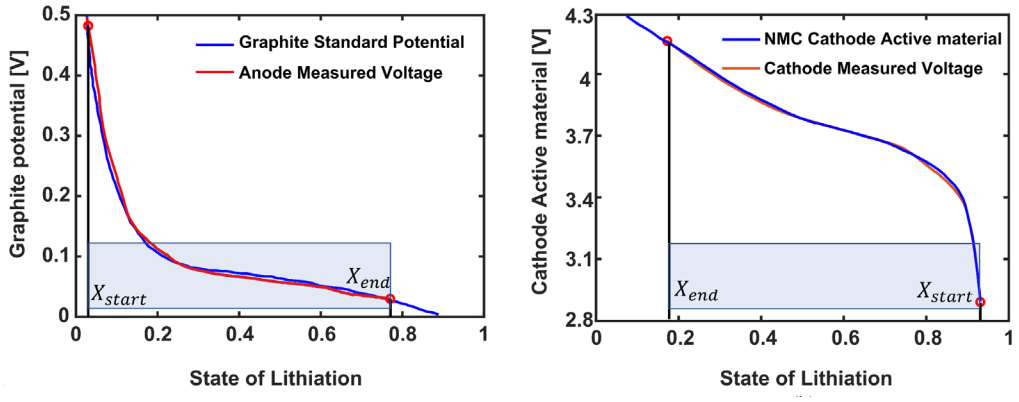

(a) (b)

Figure 3.8. Start and end points of state of lithiation of a charging cycle. Reused from [1]. Copyright Elsevier 2022

Fig. 3.8 (a) & Fig. 3.8 (b) show the difference in the state of lithiation of anode and cathode during a charging cycle.

The capacity of the electrodes is calculated by dividing the amount of charge transferred during a charging cycle by the percentage difference in the state of lithiation of each electrode. Eq. 3.7 and Eq. 3.8 state the calculation of anode and cathode capacity, respectively.

$$Q_{anode} = \frac{Q_{charge}}{X_{diff_a}} \tag{3.7}$$

$$Q_{cathode} = \frac{Q_{charge}}{X_{diff_c}} \tag{3.8}$$

where, Q_{anode}, $Q_{cathode}$, Q_{charge} represent the capacity of anode, cathode, and amount of charge transferred to the cell. X_{diff_a} and X_{diff_c} are the differences in the state of lithiation of anode and cathode during charging, respectively. In this study, the state of charge in each electrode is represented by the state of lithiation in each electrode.

3.6. Chapter Summary

This chapter discusses the developed three-electrode battery setup method, developed curve matching algorithm to get electrode internal parameters, electrode SOC and capacity calculation method, and available lithium-ion content monitoring method. The chapter starts with detailing the specification of the utilized lithium-ion battery for this research and then describes a novel three-electrode battery setup method. Unlike inserting external materials, the proposed 3-electrode battery setup technique uses the casing as the reference electrode for electrode potential measurement. An uncertain floating voltage issue is observed while using casing as a reference electrode for electrode potential measurement. Addressing this floating voltage, a curve matching algorithm is developed to calculate the electrode state of lithiation or state of charge. Further, electrode SOL is used to calculate electrode capacity and available lithium-ion content in the cell over the cycle.

Chapter 4. Anode SOC estimation and degradation monitoring via unknown input observer

4.1. Introduction

This chapter presents an experimental setup for a three-electrode battery pack. Followed by an unknown input observer design to estimate anode SOC using the floating voltage as unknown input to the model. A Thevenin equivalent battery model is presented to setup the mathematical estimation model. Then a model-based anode SOC and capacity estimation method are discussed in detail.

4.2. Experimental Setup

For this experiment, the same battery is used as mentioned in section 3.2, Sanyo UR18650AA lithium-ion 18650 cells. The nominal capacity of the single cell is 2.25 Ampere-hour (Ah), and the voltage is 3.6V. The cells were discharged to their standard discharge cut-off voltage, 2.5V, before the experimental setup. Three of these 18650 cells were connected in parallel to set up the battery pack. Thus, the nominal capacity of the battery pack is 6.75Ah, where the charge and discharge cut-off voltage remains the same as a single cell. The experiment was conducted at room temperature. Specifications of the battery are shown in Table I in section 3.2.

Three Sanyo UR18650AA cells are used for the three-electrode battery pack. The three-electrode battery is prepared following the method described in section 3.2.

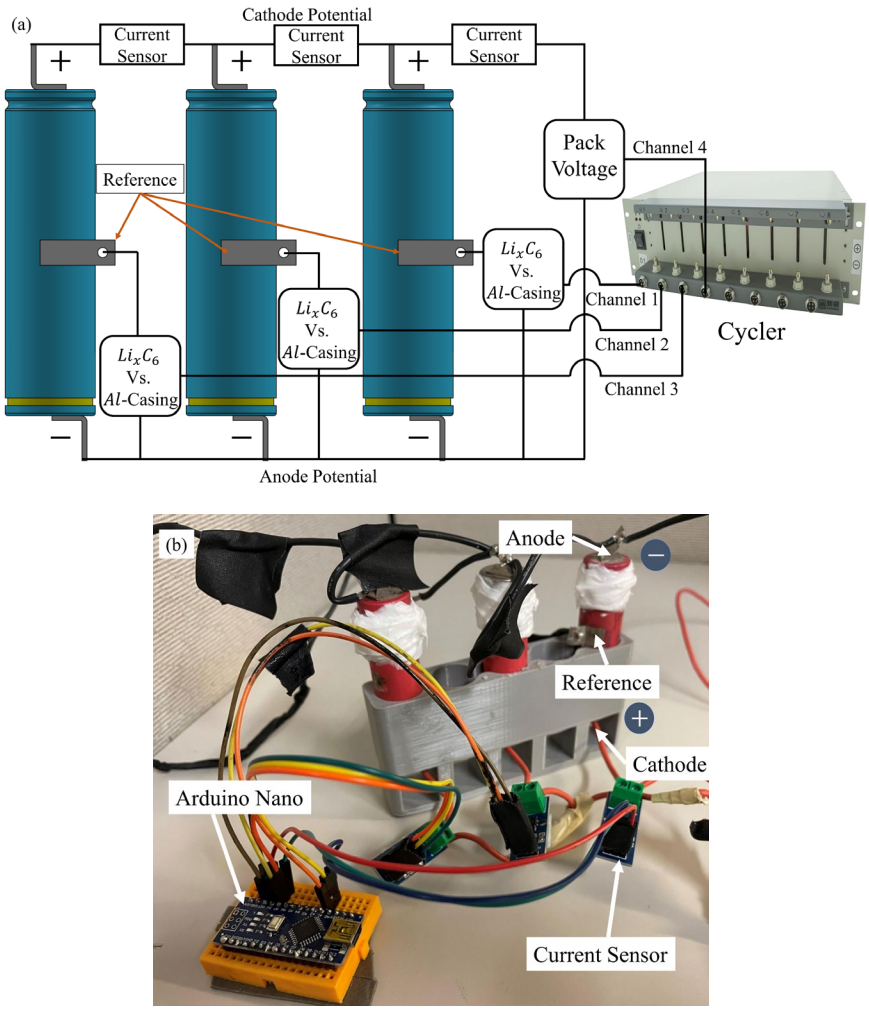

Figure 4.1. Experimental setup of three-electrode battery pack

Prepared three-electrode cells are then connected in parallel for battery pack setup. The battery pack negative and positive terminal is then connected to a channel of the cycler through cable. The reference electrode and respective anode of each cell in the pack are connected to a channel via cable to record the voltage difference between the negative terminal and that cell's reference. Three channels of the cycler are used for recording the voltage difference of the anode and reference for three cells. A current sensor is connected between each two cell's cathode connection. Further, the current sensors are connected to

an Arduino nano for recording current input through each cell. The battery pack was cycled using the standard constant-current and constant-voltage (CC-CV) charge and discharge protocol. The pack was charged and discharged with 0.7C (4725mA) current, where charge and discharge cut-off voltages were set to 4.2V and 2.5V, respectively. The charge and discharge cut-off current were set to 1/50 C (135mA). The anode voltage of each cell in the battery pack is recorded with respect to the respective reference electrode of the cell. The experimental setup of the battery pack and electrical wiring is shown in Fig. 4.1(a) and 4.1(b).

4.3. Floating Anode Potential

We noticed that the recorded anode voltage progressively increases and decreases during cycling. We call this voltage shift anode floating voltage.

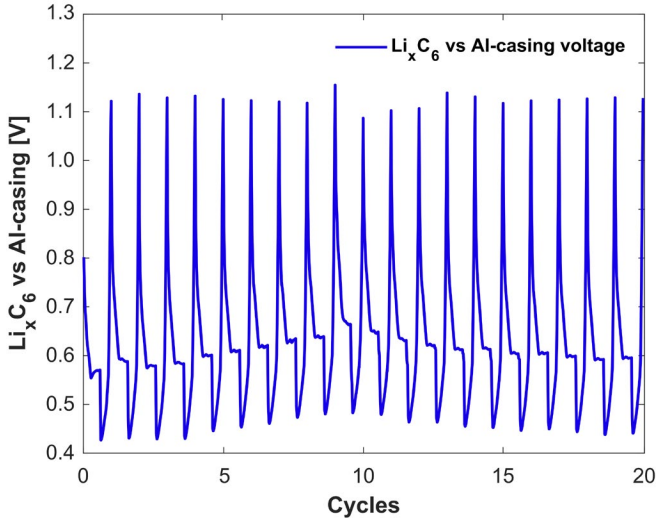

Figure 4.2. Li_xC_6 vs *Al*-casing voltage

The anode potential with respect to the reference casing is shown in Fig. 4.2. This study uses this floating voltage as the unknown input to the system as the voltage up and downshifting pattern is unknown.

4.4. Observer Design

A constant current constant voltage charging protocol is utilized to cycle the battery pack. However, due to the parallel connection, the current input to an individual cell is no longer constant. Thus, due to variable current input, a smooth anode potential curve can not be obtained. Therefore, the curve matching algorithm presented in section 3.4 no longer works as expected. Moreover, the obtained anode potential up and downshifting pattern is unknown. Thus, an unknown input observer is employed to estimate anode SOC using the floating anode potential as unknown input to the system.

To design an unknown input observer for anode SOC estimation, we considered a linear system, and the mathematical model of the system is as follows,

$$\dot{x}(t) = Ax(t) + Bu(t) + Dv(t) \tag{4.1}$$

$$y(t) = Cx(t) \tag{4.2}$$

where $x(t)$, $u(t)$, and $v(t)$ are the state vector, the input vector, the unknown input vector, and $y(t)$ is the output vector. A, B, C, and D are dynamic parameters of the considered system consisting of appropriate dimensions. Rank $(C * D)$ = rank (D) is required for the system to be observable where (C, A) is an observable pair.

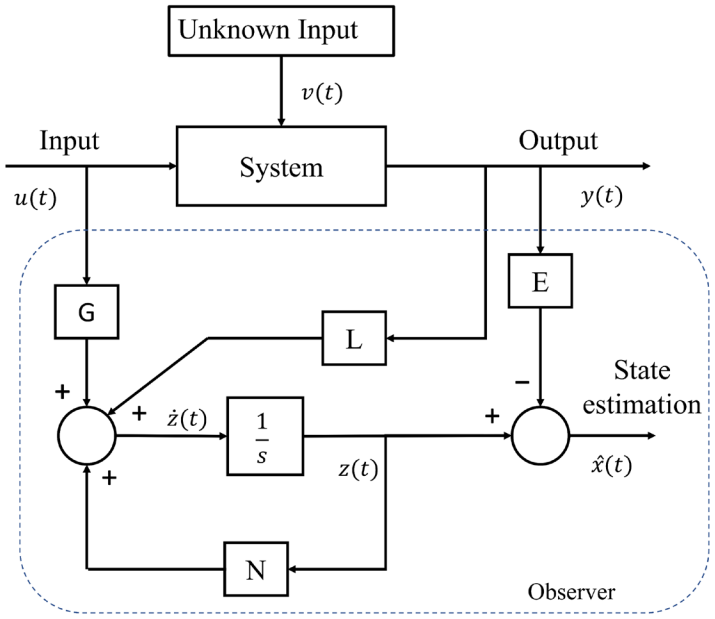

Figure 4.3. Structure of the unknown input observer

The structure of the UIO for the above-mentioned (4.1) linear system can be described as follows [79]. The structure of such UIO is shown in Fig. 4.3 [80].

$$\dot{z}(t) = Nz(t) + Ly(t) + Gu(t) \tag{4.3}$$

$$\hat{x}(t) = z(t) - Ey(t) \tag{4.4}$$

where $z(t)$ is the UIO state vector and $\hat{x}(t)$ is the estimated state vector. UIO parameter matrices are defined as N, L, $G$and E with appropriate dimensions. For the estimated state vector, $\hat{x}(t)$ convergence to $x(t)$, the UIO parameters are determined by formulating into LMI.

UIO state estimation error can be noted as follows [79],

$$e(t) = \hat{x}(t) - x(t) = z(t) - Mx(t) \tag{4.5}$$

With,

$$M = I + EC \tag{4.6}$$

where e and I are the state estimation error and the identity matrix, respectively.

Hence, state estimation error dynamics can be given as stated below [79]:

$$\dot{e}(t) = \dot{z}(t) - M\dot{x}(t) \tag{4.7}$$

Substituting $\dot{x}(t)$ and $\dot{z}(t)$ from equation (4.1) and (4.3) into equation (4.7) yields,

$$\dot{e}(t) = Nz(t) + Ly(t) + Gu(t) - M(Ax(t) + Bu(t) + Dv(t)) \tag{4.8}$$

With $e(t) = z(t) - Mx(t)$ the equation (4.8) reads as,

$$\dot{e}(t) = Ne + (NM + LC - MA)x(t)$$

$$+(G - MB)u(t)$$

$$-MDv(t) \tag{4.9}$$

To ensure that the system is independent of the unknown input and converges, the following conditions must be satisfied [79],

$$NM + LC - MA = 0 \tag{4.10}$$

$$G - MB = 0 \text{ or } G = MB \tag{4.11}$$

$$MD = 0 \tag{4.12}$$

If the above conditions satisfy the equation (4.9) yields,

$$\dot{e}(t) = Ne(t) \tag{4.13}$$

From equation (4.13), if N is stable, the system asymptotically converges.

For $K = L + NE$ the equation (4.10) can be rewritten as [81],

$$N = MA - KC \tag{4.14}$$

Thus, to solve for L using equation (4.14),

$$L = K(I + CE) - MAE \tag{4.15}$$

where I is an identity matrix with the same dimension as $C * E$.

For the considered system $C * D = 1$, which is considered a full rank. Thus, from equation (4.12),

$$E = -D(CD)^{+} + Y(I - (CD)(CD)^{+}) \tag{4.16}$$

where, $(CD)^{+} = \left((CD)^{T}(CD)\right)^{-1}(CD)^{T}$ and Y is an arbitrary matrix [79].

For notational ease equation (4.16) is rewritten as,

$$E = U + YV \tag{4.17}$$

where, $U = -D(CD)^{+}$ and $V = I - (CD)(CD)^{+}$.

A Lyapunov function $V(t) = e(t)^{T}pe(t)$ with $P > 0$ can be considered to formulate the UIO matrices into LMI to determine the matrices such that e is asymptotically stable and the system converges [79], [82].

The dynamics of the Lyapunov function can be described as [79],

$$\dot{V}(t) = e(t)^{T}(N^{T}P + PN)e(t) \tag{4.18}$$

where $N^{T}P + PN < 0$ has to satisfy for the system to converge.

With the general solution of E from equation (4.17), the LMI [82] for the UIO matrices yields,

$$\big((I+UC)A\big)^T P + P(I+UC)A$$

$$+(VCA)^T Y^T P + PY(VCA)$$

$$-C^T K^T P - PKC < 0 \tag{4.19}$$

By solving the LMI described in (4.19) $Y, K,$ and $P > 0$ matrices are determined, which is used to determine the UIO parameter matrices, $M, G, N, L,$ and E using equations (4.6), (4.11), (4.14), (4.15), and (4.17), respectively.

4.5. Thevenin Equivalent Circuit Model

A Thevenin equivalent circuit model is utilized to design the battery half-cell model. For simplicity of the model, only one Resistor-Capacitor (RC) is used to describe the polarization and diffusion effect. The utilized equivalent battery half-cell model [83] is shown in Fig. 4.4 below. In the model V_t is terminal voltage, and standard graphite potential is used as OCV, I is the current carried through the battery, and battery material resistance is represented by the ohmic resistor R_a, V_b is the voltage of the RC branch, R_b and C_b are parallel connected RC branch that describes the polarization and diffusion effect, V_f is the unknown input to the system. The electrical behavior of this equivalent battery half-cell model can be described by the following equations and the relative parameters.

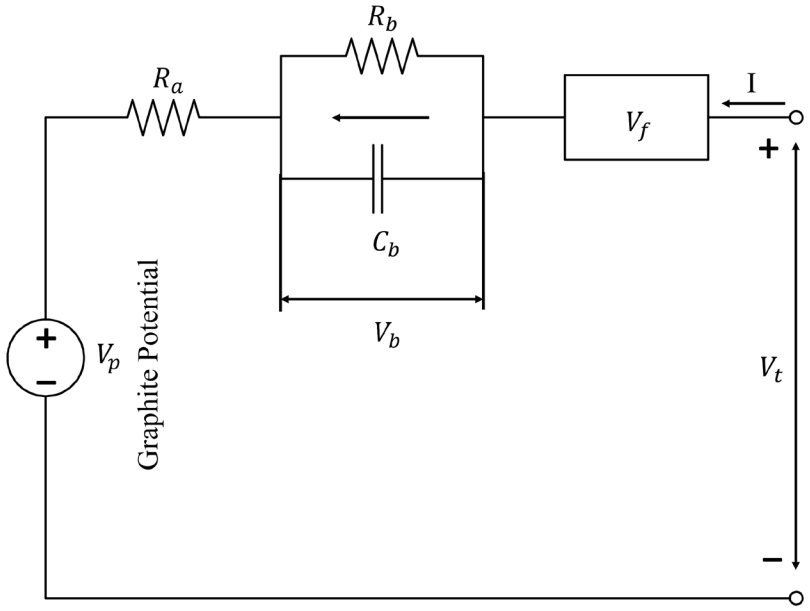

Figure 4.4. Thevenin equivalent battery half-cell model

RC branch voltage,

$$\dot{V}_b = -\frac{V_b}{R_b C_b} + \frac{I}{C_b} \tag{4.20}$$

Terminal voltage V_t is defined as

$$V_t = V_p + V_b + IR_a \tag{4.21}$$

4.6. Model Parameter Identification

The first order RC model parameters, R_a, R_b, C_b are identified by manually tuning the parameters to obtain minimum error between the estimated terminal voltage and measured anode potential. The initial guesses for the parameters are obtained from [84]. Then the parameters are tuned based on a trial and error until a minimum error value is obtained. For computational simplicity, the parameters are considered to be constant. The parameter identification results are shown in Table II.

TABLE II. Parameter identification results of the utilized model

Parameters	Symbol	Value
Cell capacity	Q_{charge}	2.22Ah
Ohmic resistance	R_a	0.012Ω
Polarization resistance	R_b	0.031Ω
Polarization capacitance	C_b	1900F

4.7. Anode SOC and Capacity Estimation

The anode SOC is estimated based on the considered linear system described in equation (4.1). System matrices A, B, C, and D can be evaluated from the equivalent battery half-cell model described above.

$$A = \begin{bmatrix} 0 & 0 \\ 0 & -\frac{1}{R_b C_b} \end{bmatrix}, B = \begin{bmatrix} \frac{1}{Q_n} \\ \frac{1}{C_b} \end{bmatrix}, D = \begin{bmatrix} 0 \\ 1 \end{bmatrix}, C = \begin{bmatrix} \frac{OCV(SOC)}{SOC} & 1 \end{bmatrix}$$

where, Q_n is the estimated anode capacity, $OCV(SOC)$ is the open-circuit voltage (standard graphite potential) as a function of SOC (state of lithiation here). As this study focuses on anode SOC estimation, the standard graphite potential and state of lithiation curve is considered as OCV-SOC characteristic curve for the anode SOC estimation. This characteristic curve is evaluated using an 11^{th}-order polynomial function as follows,

$$P(x) = P_1 x^n + P_2 x^{n-1} + \cdots + P_n x + P_{n+1} \tag{4.22}$$

where, $P_1, P_2 \ldots P_{n+1}$ are coefficients with a constant value.

Thus, the linear system (4.1) can be rewritten as,

$$\dot{x}(t) = \begin{bmatrix} 0 & 0 \\ 0 & -\frac{1}{R_b C_b} \end{bmatrix} x(t) + \begin{bmatrix} \frac{1}{Q_n} \\ \frac{1}{C_b} \end{bmatrix} u(t) + \begin{bmatrix} 0 \\ 1 \end{bmatrix} v(t) \tag{4.23}$$

and the system output vector,

$$y(t) = \begin{bmatrix} \frac{OCV(SOC)}{SOC} & 1 \end{bmatrix} x(t) \tag{4.24}$$

where system input, $u(t) = I(t)$, $y(t) = V_t(t) - I(t)R_a$, the unknown input vector, $v(t) = V_f(t)$, and the state space vector $x(t)$ has the following representation.

$$x(t) = \begin{bmatrix} SOC \\ V_b \end{bmatrix}$$

The dynamics of the SOC estimation rate can be evaluated from (4.23) as follows.

$$\dot{SOC} = \frac{1}{Q_n} \int I(t) dt \tag{4.25}$$

The algorithm to estimate SOC is shown below.

Algorithm 4.1 SOC Estimation

1: Initialize state-space vector
2: Evaluate SGP-SOL characteristic curve
3: Define system matrices, A, B, C, D
4: Solve LMI (4.19) to compute Y, K, and P > 0
5: Compute UIO matrices, M, N, L, G, and E
6: Estimate state
7: Calculate and update anode capacity

Electrode capacity is directly related to the amount of charge carried to the cell during a charging cycle. Thus, in order to calculate anode capacity, the amount of charge transferred to a single cell during a charging cycle is calculated first. Though we have adopted the CC-CV charging protocol for the battery pack cycling, the current following through, the individual battery is no longer constant in the CC part of the cycling due to parallel cell connection. Thus, the amount of charge carried out to the cell during a charging cycle is calculated by integrating current over the charging time as stated in equation (3.4).

Anode capacity is calculated by dividing the total charge transferred to the cell by the difference between the estimated end of charge SOC and the initial SOC. In this study, the SOC of the anode is represented as the state of lithiation of the anode. Anode storage capacity is calculated using equations (3.7).

4.8. Chapter Summary

This chapter presents a three-electrode battery pack setup method where the battery casing is used as a reference electrode, an unknown input observer design, and a model-based anode SOC and capacity estimation method. The chapter starts by discussing the three-electrode battery and battery pack setup alongside the experimental setup. Then to utilize the anode floating voltage for SOC estimation, an unknown input observer is employed. The anode potential randomly shifts up and down, which makes it uncertain thus, it is used as unknown input to the system. The UIO parameter matrices are expressed as a linear matrix inequality (LMI), and the parameter matrices are calculated by solving the LMI. Then using a Thevenin equivalent circuit model, a mathematical model-based anode SOC and capacity estimation method is presented. For the Thevenin equivalent battery model, unlike the open-circuit voltage, the standard graphite potential is used so that the battery model acts as a half cell.

Chapter 5. Results

5.1. Introduction

This chapter is divided into several sections to present the experimental results of both methodologies discussed in previous chapters. A brief discussion analyzes the result outcomes. The curve matching algorithm-based electrode SOC and capacity calculation method are presented first, followed by the unknown input observer-based anode SOC and capacity estimation method. Curve matching-based results include cell capacity fade, anode, cathode capacity fade, SOC calculation, and overall cell degradation discussion. Observer and model-based results consist of cell capacity fade discussion, anode SOC and capacity estimation, overall cell degradation, and a comparative study with the existing journal.

5.2. Curve Matching Results

In this section, the experimental results of the proposed method are evaluated, and cell capacity over cycles is calculated and compared with the calculated individual electrode capacity to analyze the battery degradation status. The stoichiometric range of each electrode is then visualized to calculate the lithium ions loss in the cell. The battery degradation pattern is discussed in detail to understand the overall battery degradation status. This research focuses more on developing the three-electrode battery and a method for electrode's state of charge and capacity calculation. The experimental data were collected from six three-electrode batteries and the best anode potential data among them is used as the experimental data for further calculations.

5.2.1. Cell Capacity Fade

Cell capacity is calculated using Eq. 3.5, which is compared with the individual electrode's capacity fade. Fig. 5.1 shows the cell's experimental current and voltage data along with the cell's capacity graph over cycles. From the cell capacity graph, we observe that over 80 cycles, the battery capacity decreases by 0.08Ah, which is 3.6% of the initial cell capacity. We compared the capacity fade of the three-electrode cell made by our proposed method to the conventional three-electrode setup (inserting a Li metal into the cell).

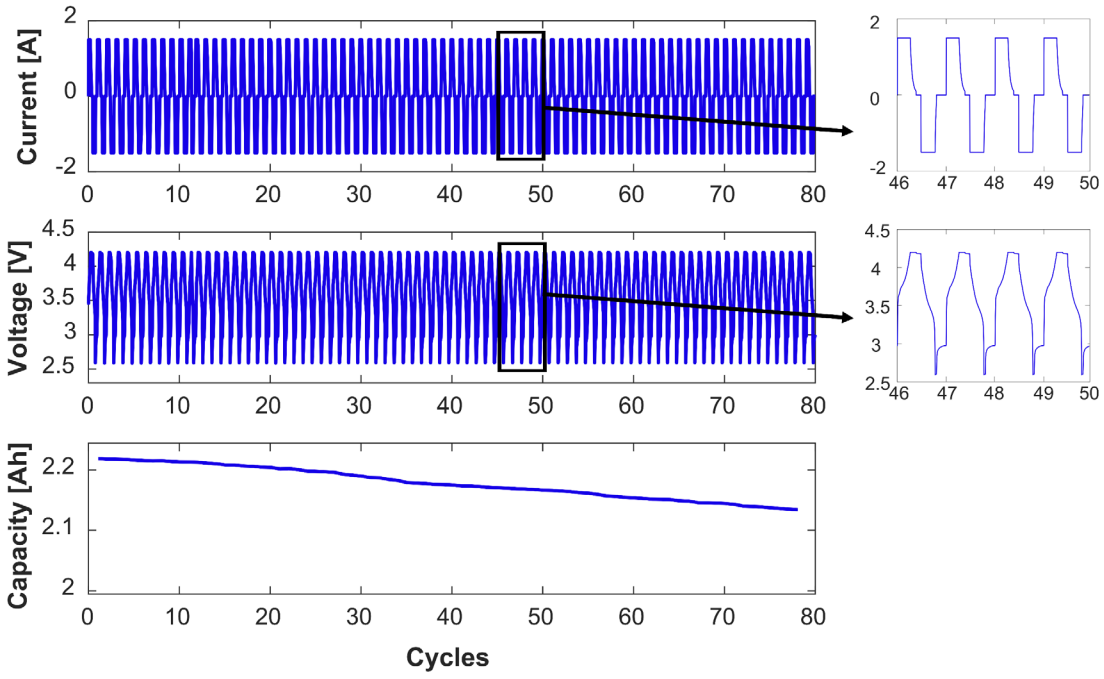

Figure 5.1. Experimental results for cell over a CCCV charge profile: current profile, measured cell voltage, capacity. Reused from [1]. Copyright Elsevier 2022

Table III shows a comparison of an average capacity fade per cycle among different three-electrode cell setups over 20 cycles. This comparison shows that using casing as reference

electrode cell capacity fade remained minimal over cycle compared to other conventional Li metal insertion methods.

TABLE III. Capacity fade comparison

The 3-electrode cell setup technique	Cell type	Average capacity loss per cycle over 20 cycles (%)
Using casing	NMC	0.032
Li metal insertion in the center [76]	NMC	0.12
Patch-modified with Li metal foil [75]	NMC	1.1227 ± 0.497
Wire-modified with Li plated copper wire [75]	NMC	0.1726 ± 0.1398

This low cell degradation suggests that the proposed three-electrode cell setup does not affect the battery's performance and can be easily adopted in the manufacturing process.

5.2.2. Anode Capacity Fade and Anode SOC

Anode capacity is calculated by dividing the amount of transferred charge to the cell during a charging cycle by the percentage difference in the state of lithiation in the anode using Eq. 3.7. Fig. 5.2 shows the anode capacity in ampere-hour (Ah) over 80 cycles. Over cycling, anode capacity decreases by 0.1Ah, about 3.2% of the initial anode capacity of 3.11Ah. This study shows that the anode capacity fade is less than the overall cell capacity fade, and the initial anode capacity is higher than that of the cell's initial capacity of 2.22Ah.

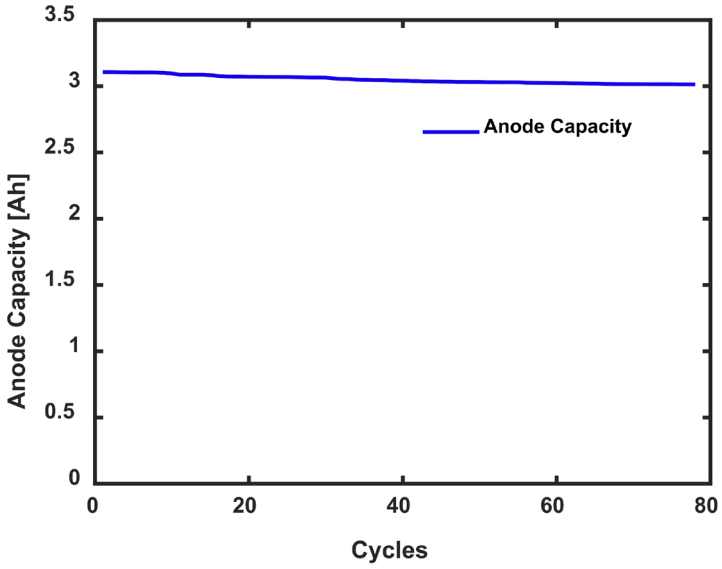

Figure 5.2. Calculated anode capacity over charging cycles. Reused from [1]. Copyright Elsevier 2022

The stoichiometric range of the anode (which is also the state of lithiation and state of charge of the anode) shows the remaining cyclable lithium ions that fill the anode capacity during a charging cycle.

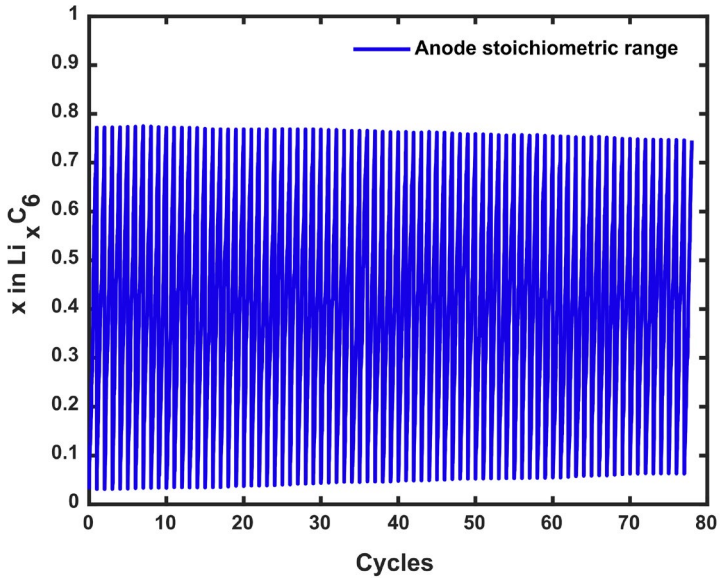

Figure 5.3. Anode stoichiometric range. Reused from [1]. Copyright Elsevier 2022

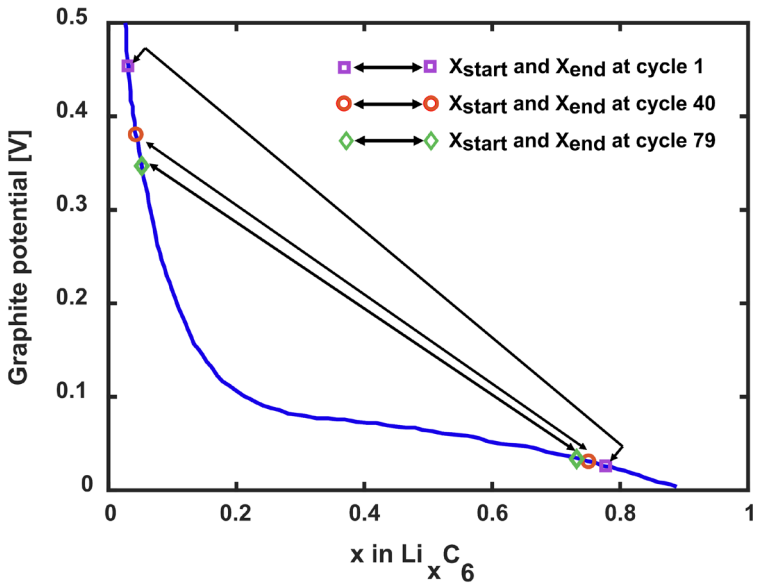

Figure 5.4. Change in stoichiometric range over charging cycles. Reused from [1]. Copyright Elsevier 2022

Fig. 5.3 shows the stoichiometric range of the anode over cycling, and Fig. 5.4 shows the anode stoichiometric range changes. We observed that the anode's initial SOC gradually increased from 2.1% to 6.4%, while the full-charge anode SOC decreased from 78.3% to 74.5%. This study shows that the stoichiometric range of the anode gradually decreases over the cycling period due to the cyclable lithium ions loss.

5.2.3. Cathode Capacity Fade and Cathode SOC

Cathode capacity is also calculated following the same method as the anode by dividing the amount of transferred charge to the cell for a charging cycle by the percentage difference in the state of lithiation of the cathode as stated in Eq. 3.8. Fig. 5.5 shows the cathode capacity in ampere-hour over 80 cycles. Over the cycling period, cathode capacity decreases by 0.29Ah, about 10.2% of the initial capacity of 2.84Ah. This study shows that cathode storage capacity decreases faster than the anode and cell capacity because the

stoichiometric range of the cathode increases while the amount of transferred charge to the cell decreases. The initial cathode storage capacity is also higher than the cell capacity by 0.62Ah but lower than the anode capacity by 0.27Ah.

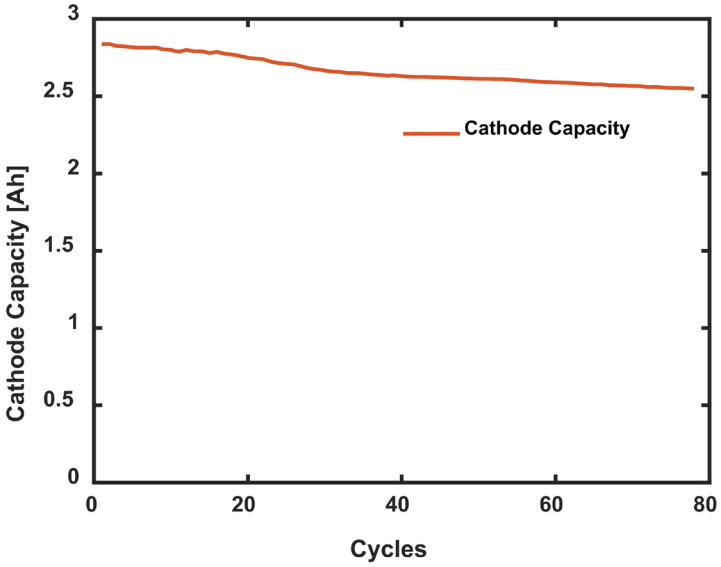

Figure 5.5. Calculated cathode capacity over charging cycles. Reused from [1]. Copyright Elsevier 2022

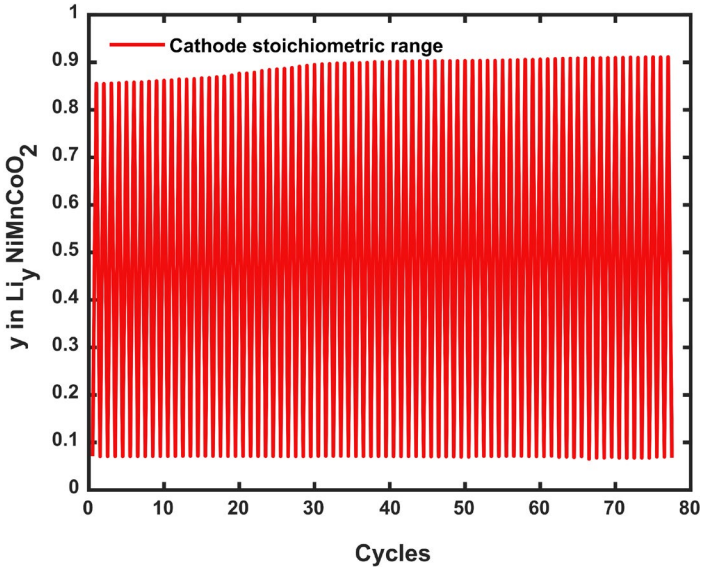

Figure 5.6. Cathode stoichiometric range. Reused from [1]. Copyright Elsevier 2022

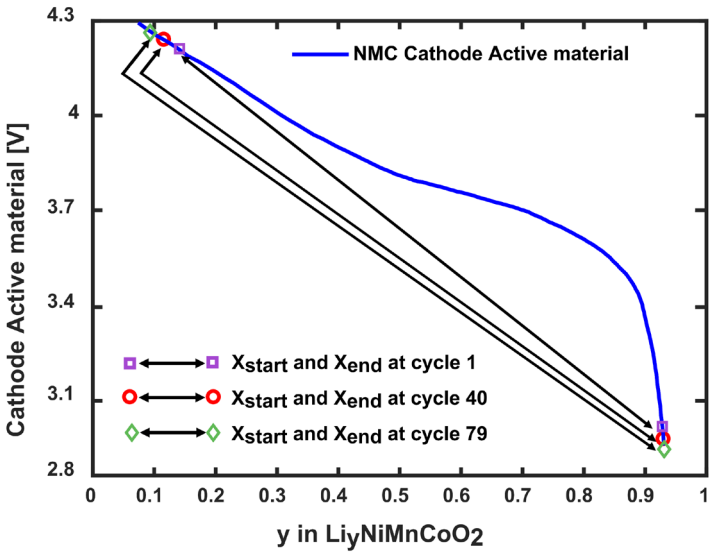

Figure 5.7. Change in stoichiometric range over charging cycles. Reused from [1]. Copyright Elsevier 2022

LII reduction pattern can be calculated by comparing the state of lithiation starting and ending points of each cycle for both electrodes. This study shows that the cathode initial SOC does not change much over the cycling period, while the end-of-charge SOC increases from 86.7% to 91.2%. Thus, we observed that the stoichiometric range of the cathode gradually increases. Fig. 5.6 shows the stoichiometric range of the cathode, and Fig. 5.7 shows the cathode stoichiometric range change over cycles.

5.2.4. Degradation Discussion

Based on the above discussion, the overall degradation patterns can be analyzed by comparing the anode, cathode, and cell capacity. As shown in Fig. 5.8, the anode capacity fade is less than the cathode and cell capacity. Cathode capacity decreases gradually as the stoichiometric range of the cathode increases while cell capacity decreases.

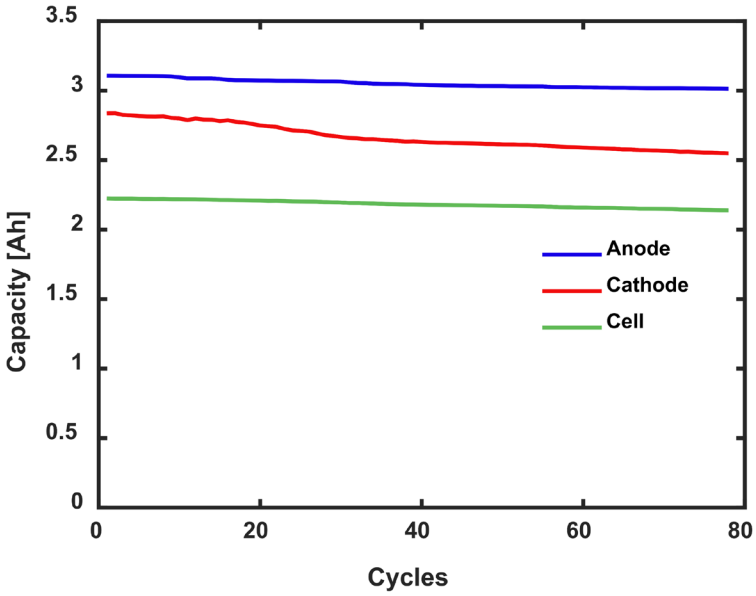

Figure 5.8. Comparison between anode (blue), cathode (red) and cell capacity (light green) . Reused from [1]. Copyright Elsevier 2022

Anode stoichiometric range decreases over the cycling period, as shown in Fig. 5.3, while the anode capacity also gradually decreases over cycles, as shown in Fig. 5.2. Fig. 5.8 shows that the cathode capacity decreases faster than the cell and anode capacity while the stoichiometric range of the cathode gradually increases, as shown in Fig. 5.6. Fig. 5.8 shows that the cell capacity is less than that of the electrodes because there are not enough lithium ions to fill the total capacity of the electrodes. A comparison between the capacity of the individual electrodes and the cell capacity shows the overall cell degradation status. The comparison shows that cell capacity decreases by 3.6%, while anode capacity decreases by 3.2%, and cathode capacity decreases by 10.2% of the initial capacity. The study shows that the initial anode capacity is about 40.1% higher than that of cell capacity, while the cathode is 27.93% higher. The state of lithiation change in each electrode shows the loss of lithium ions in the cell over the cycling period. In this study, the cathode degrades faster than the anode and cell. However, it can be different for other cells under

different operating conditions. This study presents a method to calculate electrode capacity and SOC that is very helpful in monitoring the individual electrodes' SOC. A method to monitor the cyclable lithium loss is also presented.

5.2.5. Comparison with Other Approaches

Our approach is the first one to use the battery casing as the reference electrode for electrode-level SOC and degradation monitoring. The majority of the existing methods are cell-level SOC and degradation monitoring, and our approach is on electrode-level SOC and degradation monitoring. The main differences between our approach and any existing methods are listed in Table IV.

TABLE IV. Main differences in SOC and degradation monitoring techniques

Existing methods	Our method
• Mostly for **cell-level** SOC and degradation monitoring	• **Electrode-level** SOC and degradation monitoring
• Complicated model-based estimation algorithms	• Very computational efficient curve matching algorithm
• Extremely challenging to do electrode-level SOC and degradation monitoring due to weak observability and lack of reference electrodes.	• **For the first time**, the battery casing is used as a reference electrode, so valuable information on the anode and cathode potential can be obtained, which can be used to extract internal information, including the state of charge of each electrode and its degradation status
• In research labs, some researchers in materials science inserted lithium metal into battery cells as a reference electrode, which causes safety issues (such as internal short-circuit) and consumes electrolytes (therefore degradation).	• Our method uses only battery casing, with no safety issue and no degradation issue.

- The extra inserted lithium metal electrode will significantly complicate the manufacturing process, which is not practical and not safe in actual applications
- It needs only a small gap in the battery casing, almost no changes to the manufacturing process, very practical approach

5.3. Unknown Input Observer Results

Anode SOC estimation result is evaluated in this section. We calculated cell capacity over cycles using the coulomb counting method and compared it with the anode capacity. Anode SOC and capacity fade are then discussed, followed by a detailed discussion on the battery degradation based on the capacity fade.

5.3.1. Cell Capacity Fade

The individual cell capacity in the battery pack is calculated using equation (3.4). Fig. 5.9 shows the CCCV current profile of the battery pack along with the voltage graph.

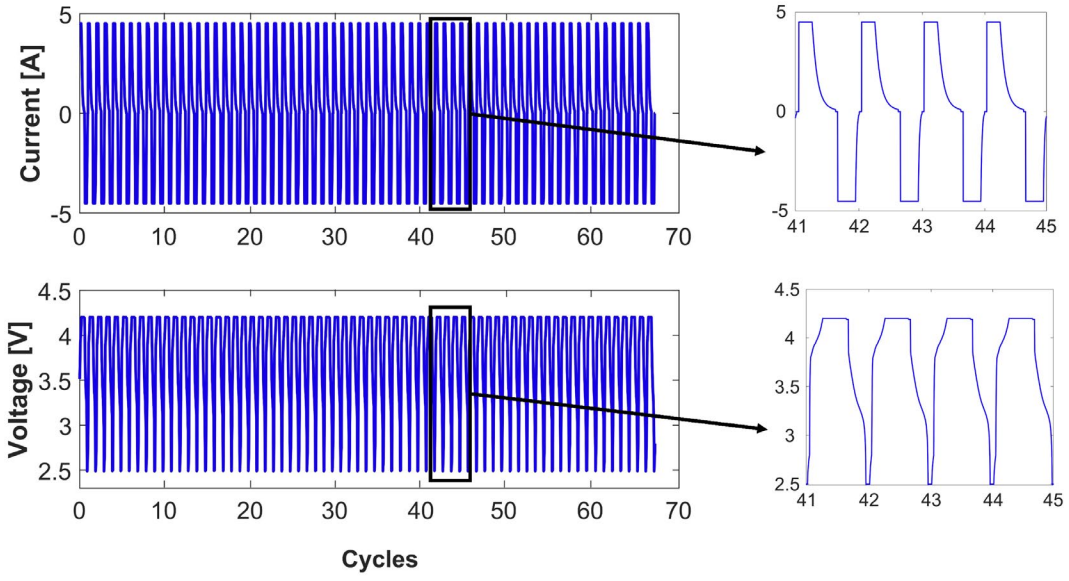

Figure 5.9. Experimental results of the battery pack over a CCCV charge profile: current profile, measured voltage

0.7C current was applied for both charging and discharging the battery pack. Though we have adopted a CCCV charging profile for this study, due to parallel cell connection, the measured current through individual cells does not have a CC part in the charging cycle.

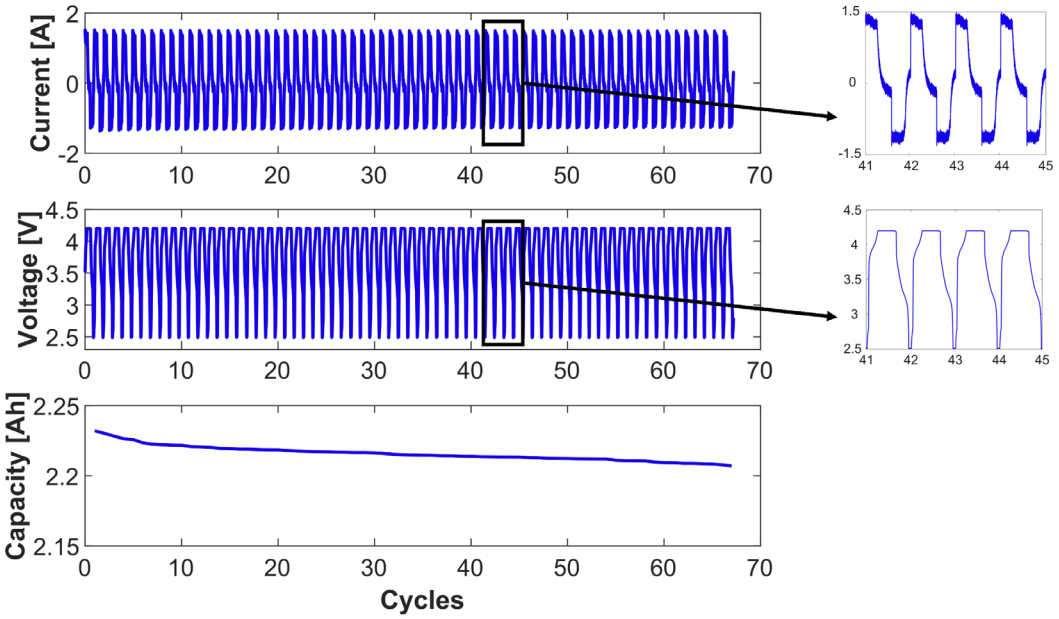

Figure 5.10. Experimental results of an individual cell in the battery pack over a variable current charge profile: current profile, measured cell voltage, capacity

An individual cell charging cycle is shown in Fig. 5.10. We see that the current profile has the shape of a CCCV charging profile, but a lot of fluctuation is observed for both the CC and CV part of charging. This variable current was induced by the current sensor and the variable current is directly used as input to the system for anode SOC estimation. Fig. 5.10 shows the variable charging profile of the individual cell in the battery pack, cell voltage, and capacity graph of the cell. Over the 68 charging cycles, the cell capacity decreases by 0.06Ah, which is 2.7% of the initial cell capacity.

5.3.2. 3-electrode Cell vs. Fresh Cell Capacity Fade

We compared the capacity fade of the fresh cell to the proposed 3-electrode cell to demonstrate the effect of the proposed 3-electrode cell setup on battery performance. Fig. 5.11 shows that the 3-electrode cell slightly degrades more than the fresh cell. The fresh cell capacity degrades by 0.03Ah which is 2.6% of the initial capacity over the 80 cycles, whereas the 3-electrode cell capacity degrades by 0.08Ah which is 3.6% of the initial capacity. Based on the capacity comparison, the proposed 3-electrode cell setup does not significantly affect cell performance.

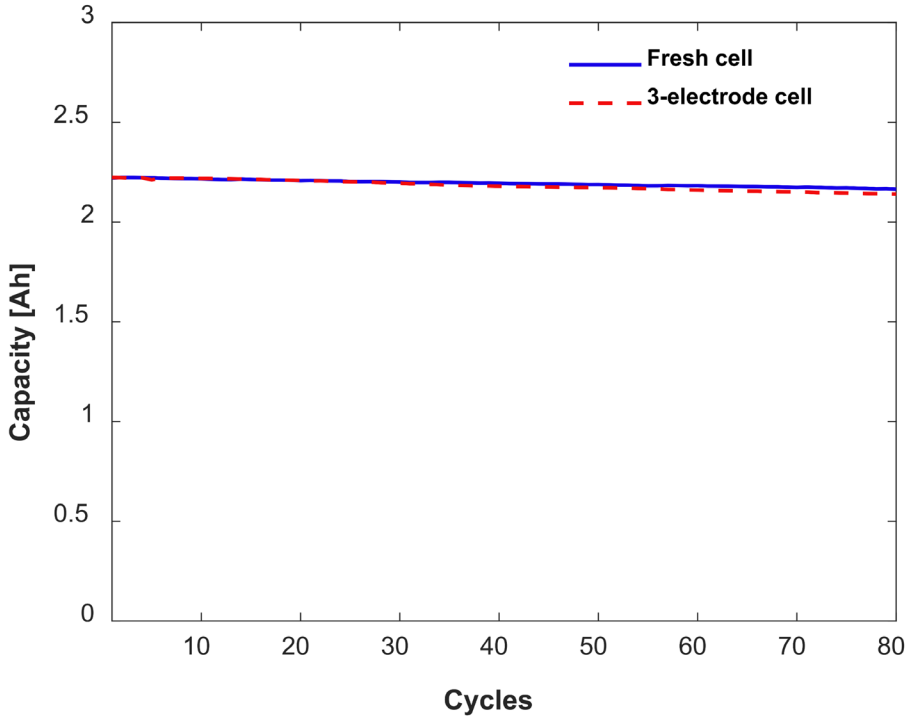

Figure 5.11. Comparison between fresh cell and 3-electrode cell capacity fade

5.3.3. Anode Capacity Fade and Anode SOC

Anode SOC is estimated using the UIO by observing the state estimation vector $\hat{x}(t)$. This study shows that the estimated full charge SOC gradually decreases from 72.85% to 65.40%, and the initial guess for SOC in the state-space vector is set to 20%, also an initial guess for anode capacity is made to be the cell initial capacity 2.22Ah.

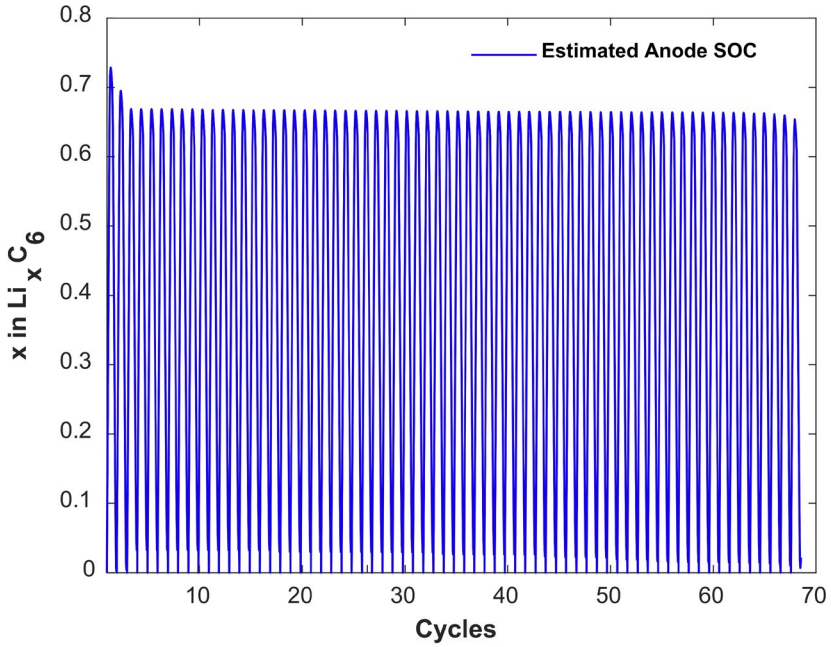

Figure 5.12. Estimated anode SOC or stoichiometric range

Estimated anode SOC is shown in Fig. 5.12. From the anode SOC graph, we see that the initial SOC starts with a high value and then gradually stabilizes to a consistent upper value. The reason behind this initial high SOC is the initial anode capacity guess for estimation. After each cycle, the anode capacity for that cycle is calculated using equation (3.7), and the system matrix, B is updated with the estimated anode capacity. The anode capacity is always higher than the cell capacity thus, the SOC estimation rate described in equation (4.25) reduces after the estimated anode capacity update. The anode SOC can also be

considered as stoichiometric range or state of lithiation of the anode. We observed that the stoichiometric range of the anode decreases over the charging cycle due to cyclable lithium loss in the cell. The capacity of the anode is calculated by dividing the total charge carried to the cell in a charging cycle by the percentage difference of the estimated state of lithiation of the anode after each cycle, as stated in equation (3.7). The calculated anode

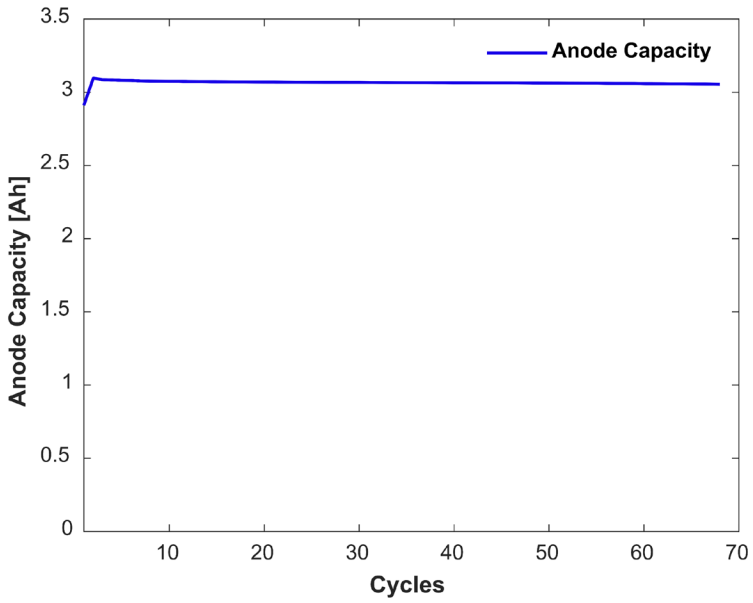

Figure 5.13. Anode capacity graph over cycles

capacity over 68 cycles is shown in Fig. 5.13. From the figure, we see the initial anode capacity is much lower than the next cycle capacity. This is because the initial capacity guess for estimation is the cell capacity which is much smaller than the anode capacity and the initial SOC end-of-charge value is very high compared to the other cycles. Thus, from equation (3.7) the difference between the end of charge SOC and the start of charge SOC is a higher number. Dividing the initial guess for anode capacity by this higher number produces a smaller anode capacity estimation value. This is why the initial anode capacity

starts with a smaller number as shown in Fig. 5.13. This study shows that anode capacity decreases by 0.062 Ah over 68 cycles which is 2.15% of the mean anode capacity of 2.88 Ah. We observed that anode capacity fade is less than the overall cell capacity fade by 1.27%. We also noticed that the anode capacity is higher than the cell capacity because there are not enough lithium ions to fill the total capacity of the anode [1].

5.3.4. Degradation Discussion

Based on the capacity fade discussion of anode and cell, we can see the overall degradation pattern of the cell, which states that anode capacity is much higher than the cell capacity, and over time, the anode degrades slower than the cell. This could be due to the much higher anode storage capacity compared to cell capacity. A comparison between the anode and cell capacity fade is shown in Fig. 5.14 below. Fig. 5.12 and 5.13 shows that anode capacity decreases gradually while the stoichiometric range (or SOC) also decreases. This is because the cell charge carrying capacity decreases faster, possibly due to various cell degradation mechanisms and cyclable lithium-ion loss. Fig. 5.14 shows that cell storage capacity is always less than the anode storage capacity because there are not enough lithium ions in the cell to fill the anode's remaining capacity [1]. This study presents an anode SOC estimation method utilizing the variable current and the anode floating voltage as an unknown input to the system. A three-electrode battery pack setup is also presented that helps monitor an individual battery's internal parameters.

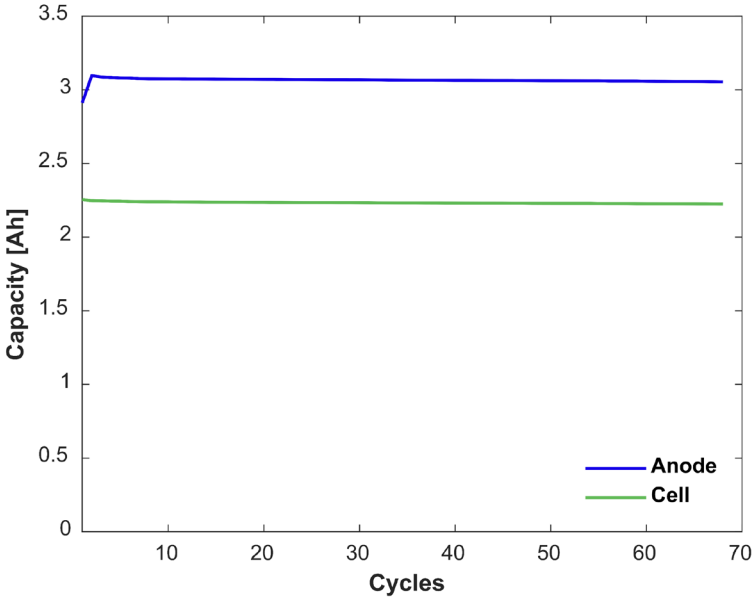

Figure 5.14. Comparison between anode (blue) and cell capacity (light green)

5.3.5. Comparison to the Existing Research

To evaluate the accuracy of the designed observer, we have compared the estimated anode and cell capacity to the calculated capacity and the estimated anode SOC to the anode SOC presented in [1]. From Fig. 5.15, we see that the estimated anode SOC is similar to the one presented in [1] with an estimation error of 5.33%. The estimated mean anode capacity for the single-cell varies by 0.21Ah from the calculated value of the reference [1]. This could be due to the initial SOC estimated by the herein proposed method, which is close to ZERO at the beginning of each cycle. However, this value is not always zero, as presented in [1]. Fig. 5.16 shows the anode capacity comparison between the estimated value and the calculated value from [1].

TABLE V. Capacity comparison to the existing works

Initial Capacity	Estimated (Ah)	Calculated (Ah)
Cell Type	UR18650AA. Sanyo	UR18650AA. Sanyo
Cell	2.22	2.22
Anode	2.88	3.09

The capacity comparison in Table V shows that the cell capacity is the same as the reference [1] while the anode capacity varies by 0.21Ah with an estimation error of 6.7%.

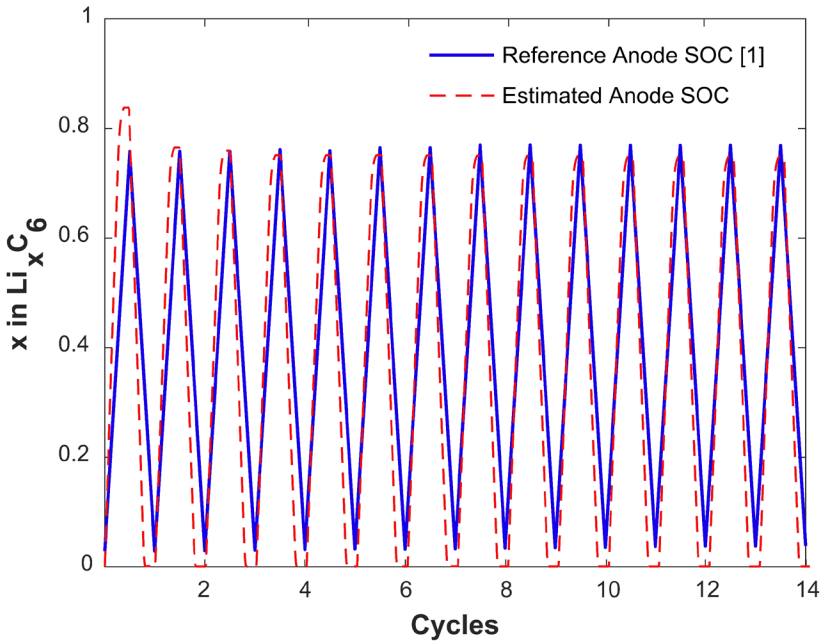

Figure 5.15. Comparison between estimated anode SOC and the reference anode SOC form for standard CCCV charging profile for a single three-electrode cell

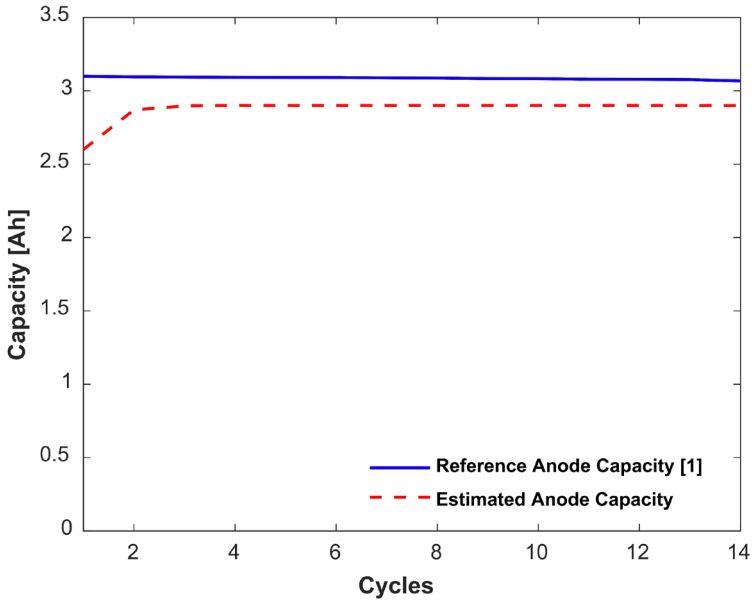

Figure 5.16. Comparison between estimated anode capacity and the reference anode capacity form for standard CCCV charging profile for a single three-electrode cell

5.4. Chapter Summary

This chapter presents the experimental results of the electrode SOC and degradation monitoring methodologies presented in this thesis. The results are discussed in detail to demonstrate the outcome. The chapter presents the results of the curve matching-based electrode SOC and degradation monitoring method followed by the unknown input observer-based anode SOC estimation and degradation monitoring method results. In the curve matching-based results, cell, anode, and cathode capacity fade are discussed. A comparison between cell and electrode capacity fade is also illustrated to analyze overall cell degradation and electrode contribution to it. The anode and cathode state of charge and change in stoichiometric range over charging cycles is demonstrated. In unknown input, observer-based results anode and cell capacity fade are discussed. The estimated anode SOC is presented. Further, the accuracy of the developed model is evaluated by comparing

the results to the existing journals. The capacity fade of the fresh cell is compared to the proposed 3-electrode cell to demonstrate the effect of the proposed 3-electrode cell setup on battery performance.

Chapter 6. Conclusion and Future Work

6.1. Conclusion

The increasing demand for electric vehicles and other electric devices that are vastly powered by a lithium-ion battery poses a concern about the reusability of a large number of retired EV batteries. The Li-ion battery performance improvement or second-life usability assessment highly depends on battery internal parameter monitoring such as electrode state of charge and capacity also available cyclable lithium-ions in the cell. Knowing these internal parameters will help battery performance improvement through optimization and classify these batteries for further use or recycling. This thesis presents a novel method to set up a three-electrode battery and a three-electrode battery pack using a battery casing as the reference electrode. Further, a curve matching algorithm is developed to calculate the state of charge of both electrodes and the degradation status (including the storage capacity fade of each electrode and the total cyclable lithium in the battery), and an unknown input observer-based estimation method is presented to estimate the anode SOC of an individual battery in the battery pack for variable current input. An electrode capacity calculation and an anode capacity calculation method are described using the calculated SOC and estimated anode SOC, respectively. Comparing the electrode capacity to the cell capacity, the battery's overall degradation is demonstrated.

The proposed innovative approach uses the battery casing as a reference electrode to provide the battery's internal state in real-time. By using battery casing as the reference, this innovative approach overcomes the limitation of other insertion methods (adding extra metal or material to battery cells, which causes safety issues and additional manufacturing complexity). To solve the electrode floating voltage issue, we proposed a voltage curve

matching algorithm that is simple yet competent in understanding internal battery parameters. Further, an unknown input observer is designed for anode SOC estimation by utilizing the anode potential for variable current profile. The results achieved are incredible to monitor each electrode's SOC and capacity fade and cyclable lithium loss in the cell that can be employed to analyze the overall degradation of the battery.

In conclusion, the proposed methods introduce an innovative solution for lithium-ion battery electrode parameter estimation which can be implemented in practical application with further improvement in the algorithm. The proposed reference electrode setup method may solve the existing reference electrode drawbacks in the field.

6.2. Recommendations for Future Work

With regards to the curve matching algorithm, a dynamic load-based experimental setup should be considered. This will evaluate the 3-electrode cell performance for practical application and its usability in practical applications.

With regards to the observer-based SOC estimation method, cathode SOC and capacity fade also should be considered for estimation to better evaluate the battery degradation.

References

[1] A. Rahman and X. Lin, "Li-ion battery individual electrode state of charge and degradation monitoring using battery casing through auto curve matching for standard CCCV charging profile," *Applied Energy*, vol. 321, p. 119367, Sep. 2022, doi: 10.1016/j.apenergy.2022.119367.

[2] A. Rahman, X. Lin, and C. Wang, "Li-Ion Battery Anode State of Charge Estimation and Degradation Monitoring Using Battery Casing via Unknown Input Observer," *Energies (Basel)*, vol. 15, no. 15, p. 5662, Aug. 2022, doi: 10.3390/en15155662.

[3] X. Hu, L. Xu, X. Lin, and M. Pecht, "Battery Lifetime Prognostics," *Joule*, vol. 4, no. 2, Feb. 2020, doi: 10.1016/j.joule.2019.11.018.

[4] A. Cordoba-Arenas, S. Onori, Y. Guezennec, and G. Rizzoni, "Capacity and power fade cycle-life model for plug-in hybrid electric vehicle lithium-ion battery cells containing blended spinel and layered-oxide positive electrodes," *Journal of Power Sources*, vol. 278, pp. 473–483, Mar. 2015, doi: 10.1016/J.JPOWSOUR.2014.12.047.

[5] W.-Y. Chang, "The State of Charge Estimating Methods for Battery: A Review," *ISRN Applied Mathematics*, vol. 2013, pp. 1–7, Jul. 2013, doi: 10.1155/2013/953792.

[6] M. Dubarry, C. Truchot, and B. Y. Liaw, "Synthesize battery degradation modes via a diagnostic and prognostic model," *Journal of Power Sources*, vol. 219, pp. 204–216, Dec. 2012, doi: 10.1016/J.JPOWSOUR.2012.07.016.

[7] I. Bloom *et al.*, "Differential voltage analyses of high-power, lithium-ion cells: 1. Technique and application," *Journal of Power Sources*, vol. 139, no. 1–2, pp. 295–303, Jan. 2005, doi: 10.1016/J.JPOWSOUR.2004.07.021.

[8] C. R. Birkl, M. R. Roberts, E. McTurk, P. G. Bruce, and D. A. Howey, "Degradation diagnostics for lithium ion cells," *Journal of Power Sources*, vol. 341, pp. 373–386, Feb. 2017, doi: 10.1016/J.JPOWSOUR.2016.12.011.

[9] E. Sarasketa-Zabala, F. Aguesse, I. Villarreal, L. M. Rodriguez-Martinez, C. M. López, and P. Kubiak, "Understanding Lithium Inventory Loss and Sudden Performance Fade in Cylindrical Cells during Cycling with Deep-Discharge Steps," *The Journal of Physical Chemistry C*, vol. 119, no. 2, Jan. 2015, doi: 10.1021/jp510071d.

[10] J. Tian, R. Xiong, W. Shen, and F. Sun, "Electrode ageing estimation and open circuit voltage reconstruction for lithium ion batteries," *Energy Storage Materials*, vol. 37, pp. 283–295, May 2021, doi: 10.1016/j.ensm.2021.02.018.

[11] S. J. An, J. Li, C. Daniel, D. Mohanty, S. Nagpure, and D. L. Wood, "The state of understanding of the lithium-ion-battery graphite solid electrolyte interphase (SEI) and its relationship to formation cycling," *Carbon N Y*, vol. 105, Aug. 2016, doi: 10.1016/j.carbon.2016.04.008.

[12] M.-T. F. Rodrigues, F. N. Sayed, H. Gullapalli, and P. M. Ajayan, "High-temperature solid electrolyte interphases (SEI) in graphite electrodes," *Journal of Power Sources*, vol. 381, Mar. 2018, doi: 10.1016/j.jpowsour.2018.01.070.

[13] C. R. Birkl, M. R. Roberts, E. McTurk, P. G. Bruce, and D. A. Howey, "Degradation diagnostics for lithium ion cells," *Journal of Power Sources*, vol. 341, pp. 373–386, Feb. 2017, doi: 10.1016/J.JPOWSOUR.2016.12.011.

[14] X. Han, M. Ouyang, L. Lu, J. Li, Y. Zheng, and Z. Li, "A comparative study of commercial lithium ion battery cycle life in electrical vehicle: Aging mechanism identification," *Journal of Power Sources*, vol. 251, pp. 38–54, Apr. 2014, doi: 10.1016/J.JPOWSOUR.2013.11.029.

[15] D. Aurbach, B. Markovsky, Y. Talyossef, G. Salitra, H.-J. Kim, and S. Choi, "Studies of cycling behavior, ageing, and interfacial reactions of LiNi0.5Mn1.5O4 and carbon electrodes for lithium-ion 5-V cells," *Journal of Power Sources*, vol. 162, no. 2, pp. 780–789, Nov. 2006, doi: 10.1016/j.jpowsour.2005.07.009.

[16] B. Xu, A. Oudalov, A. Ulbig, G. Andersson, and D. S. Kirschen, "Modeling of Lithium-Ion Battery Degradation for Cell Life Assessment," *IEEE Transactions on Smart Grid*, vol. 9, no. 2, Mar. 2018, doi: 10.1109/TSG.2016.2578950.

[17] J. Li, K. Adewuyi, N. Lotfi, R. G. Landers, and J. Park, "A single particle model with chemical/mechanical degradation physics for lithium ion battery State of Health (SOH) estimation," *Applied Energy*, vol. 212, Feb. 2018, doi: 10.1016/j.apenergy.2018.01.011.

[18] X. Lin, K. Khosravinia, X. Hu, J. Li, and W. Lu, "Lithium Plating Mechanism, Detection, and Mitigation in Lithium-Ion Batteries," *Progress in Energy and Combustion Science*, vol. 87, p. 100953, Nov. 2021, doi: 10.1016/J.PECS.2021.100953.

[19] D. J. G. Ives, G. J. Janz, and C. v. King, "Reference Electrodes: Theory and Practice," *Journal of The Electrochemical Society*, vol. 108, no. 11, 1961, doi: 10.1149/1.2427957.

[20] R. Raccichini, M. Amores, and G. Hinds, "Critical review of the use of reference electrodes in li-ion batteries: A diagnostic perspective," *Batteries*, vol. 5, no. 1. MDPI Multidisciplinary Digital Publishing Institute, Mar. 01, 2019. doi: 10.3390/batteries5010012.

[21] M. Klett *et al.*, “Electrode Behavior RE-Visited: Monitoring Potential Windows, Capacity Loss, and Impedance Changes in $Li_{1.03}(Ni_{0.5}Co_{0.2}Mn_{0.3})_{0.97}O_2$ /Silicon-Graphite Full Cells,” *Journal of The Electrochemical Society*, vol. 163, no. 6, pp. A875–A887, Mar. 2016, doi: 10.1149/2.0271606jes.

[22] G. Nagasubramanian and D. H. Doughty, “18650 Li-ion cells with reference electrode and in situ characterization of electrodes,” *Journal of Power Sources*, vol. 150, no. 1–2, pp. 182–186, Oct. 2005, doi: 10.1016/J.JPOWSOUR.2005.02.024.

[23] S. J. An, J. Li, C. Daniel, S. Kalnaus, and D. L. Wood, “Design and Demonstration of Three-Electrode Pouch Cells for Lithium-Ion Batteries,” *Journal of The Electrochemical Society*, vol. 164, no. 7, pp. A1755–A1764, Jun. 2017, doi: 10.1149/2.0031709jes.

[24] J. R. Belt, D. M. Bernardi, and V. Utgikar, “Development and Use of a Lithium-Metal Reference Electrode in Aging Studies of Lithium-Ion Batteries,” *Journal of The Electrochemical Society*, vol. 161, no. 6, pp. A1116–A1126, May 2014, doi: 10.1149/2.062406jes.

[25] M. Dollé, F. Orsini, A. S. Gozdz, and J.-M. Tarascon, “Development of Reliable Three-Electrode Impedance Measurements in Plastic Li-Ion Batteries,” *Journal of The Electrochemical Society*, vol. 148, no. 8, p. A851, 2001, doi: 10.1149/1.1381071.

[26] M. U. Cuma and T. Koroglu, “A comprehensive review on estimation strategies used in hybrid and battery electric vehicles,” *Renewable and Sustainable Energy Reviews*, vol. 42, pp. 517–531, Feb. 2015, doi: 10.1016/j.rser.2014.10.047.

[27] A. Farmann, W. Waag, A. Marongiu, and D. U. Sauer, “Critical review of on-board capacity estimation techniques for lithium-ion batteries in electric and hybrid electric vehicles,” *Journal of Power Sources*, vol. 281, pp. 114–130, May 2015, doi: 10.1016/j.jpowsour.2015.01.129.

[28] M. Farag, M. Fleckenstein, and S. R. Habibi, “Li-Ion Battery SOC Estimation Using Non-Linear Estimation Strategies Based on Equivalent Circuit Models,” Apr. 2014. doi: 10.4271/2014-01-1849.

[29] H. He, R. Xiong, and J. Fan, “Evaluation of Lithium-Ion Battery Equivalent Circuit Models for State of Charge Estimation by an Experimental Approach,” *Energies (Basel)*, vol. 4, no. 4, Mar. 2011, doi: 10.3390/en4040582.

[30] W.-Y. Chang, “The State of Charge Estimating Methods for Battery: A Review,” *ISRN Applied Mathematics*, vol. 2013, Jul. 2013, doi: 10.1155/2013/953792.

[31] K. S. Ng, C.-S. Moo, Y.-P. Chen, and Y.-C. Hsieh, “Enhanced coulomb counting method for estimating state-of-charge and state-of-health of

lithium-ion batteries," *Applied Energy*, vol. 86, no. 9, Sep. 2009, doi: 10.1016/j.apenergy.2008.11.021.

[32] M. A. Hannan, M. S. H. Lipu, A. Hussain, and A. Mohamed, "A review of lithium-ion battery state of charge estimation and management system in electric vehicle applications: Challenges and recommendations," *Renewable and Sustainable Energy Reviews*, vol. 78, pp. 834–854, Oct. 2017, doi: 10.1016/j.rser.2017.05.001.

[33] P. A. Topan, M. N. Ramadan, G. Fathoni, A. I. Cahyadi, and O. Wahyunggoro, "State of Charge (SOC) and State of Health (SOH) estimation on lithium polymer battery via Kalman filter," in *2016 2nd International Conference on Science and Technology-Computer (ICST)*, Oct. 2016, pp. 93–96. doi: 10.1109/ICSTC.2016.7877354.

[34] X. Lai, Y. Zheng, and T. Sun, "A comparative study of different equivalent circuit models for estimating state-of-charge of lithium-ion batteries," *Electrochimica Acta*, vol. 259, Jan. 2018, doi: 10.1016/j.electacta.2017.10.153.

[35] V. Pop, H. J. Bergveld, P. H. L. Notten, and P. P. L. Regtien, "State-of-the-art of battery state-of-charge determination," *Measurement Science and Technology*, vol. 16, no. 12, Dec. 2005, doi: 10.1088/0957-0233/16/12/R01.

[36] S. Lee, J. Kim, J. Lee, and B. H. Cho, “State-of-charge and capacity estimation of lithium-ion battery using a new open-circuit voltage versus state-of-charge,” *Journal of Power Sources*, vol. 185, no. 2, Dec. 2008, doi: 10.1016/j.jpowsour.2008.08.103.

[37] Y. Song, M. Park, M. Seo, and S. W. Kim, “Improved SOC estimation of lithium-ion batteries with novel SOC-OCV curve estimation method using equivalent circuit model,” *2019 4th International Conference on Smart and Sustainable Technologies, SpliTech 2019*, Jun. 2019, doi: 10.23919/SPLITECH.2019.8783149.

[38] Yan Ma, Xiuwen Zhou, Bingsi Li, and Hong Chen, “Fractional modeling and SOC estimation of lithium-ion battery,” *IEEE/CAA Journal of Automatica Sinica*, vol. 3, no. 3, Jul. 2016, doi: 10.1109/JAS.2016.7508803.

[39] D. Andre, C. Appel, T. Soczka-Guth, and D. U. Sauer, “Advanced mathematical methods of SOC and SOH estimation for lithium-ion batteries,” *Journal of Power Sources*, vol. 224, Feb. 2013, doi: 10.1016/j.jpowsour.2012.10.001.

[40] A. Bartlett, J. Marcicki, S. Onori, G. Rizzoni, X. G. Yang, and T. Miller, “Electrochemical Model-Based State of Charge and Capacity Estimation for a Composite Electrode Lithium-Ion Battery,” *IEEE*

Transactions on Control Systems Technology, 2015, doi: 10.1109/TCST.2015.2446947.

[41] X. Tang, B. Liu, and F. Gao, "State of Charge Estimation of LiFePO 4 Battery Based on a Gain-classifier Observer," *Energy Procedia*, vol. 105, May 2017, doi: 10.1016/j.egypro.2017.03.585.

[42] M. Wei, M. Ye, J. B. Li, Q. Wang, and X. X. Xu, "State of charge estimation for lithium-ion batteries using dynamic neural network based on sine cosine algorithm:," *https://doi.org/10.1177/09544070211018038*, vol. 236, no. 2–3, pp. 241–252, May 2021, doi: 10.1177/09544070211018038.

[43] X. Chen, X. Chen, and X. Chen, "A novel framework for lithium-ion battery state of charge estimation based on Kalman filter Gaussian process regression," *International Journal of Energy Research*, vol. 45, no. 9, pp. 13238–13249, Jul. 2021, doi: 10.1002/er.6649.

[44] L. Haoran, L. Liangdong, Z. Xiaoyin, and S. Mingxuan, "Lithium Battery SOC Estimation Based on Extended Kalman Filtering Algorithm," in *2018 IEEE 4th International Conference on Control Science and Systems Engineering (ICCSSE)*, Aug. 2018, pp. 231–235. doi: 10.1109/CCSSE.2018.8724766.

[45] W. Junping, G. Jingang, and D. Lei, “An adaptive Kalman filtering based State of Charge combined estimator for electric vehicle battery pack,” *Energy Conversion and Management*, vol. 50, no. 12, pp. 3182–3186, Dec. 2009, doi: 10.1016/J.ENCONMAN.2009.08.015.

[46] P. Shrivastava, T. K. Soon, M. Y. I. bin Idris, and S. Mekhilef, “Overview of model-based online state-of-charge estimation using Kalman filter family for lithium-ion batteries,” *Renewable and Sustainable Energy Reviews*, vol. 113, p. 109233, Oct. 2019, doi: 10.1016/j.rser.2019.06.040.

[47] M. A. Rahman, S. Anwar, and A. Izadian, “Electrochemical model parameter identification of a lithium-ion battery using particle swarm optimization method,” *Journal of Power Sources*, vol. 307, Mar. 2016, doi: 10.1016/j.jpowsour.2015.12.083.

[48] W. Sung and C. B. Shin, “Electrochemical model of a lithium-ion battery implemented into an automotive battery management system,” *Computers & Chemical Engineering*, vol. 76, May 2015, doi: 10.1016/j.compchemeng.2015.02.007.

[49] N. Yang, X. Zhang, and G. Li, “State-of-charge estimation for lithium ion batteries via the simulation of lithium distribution in the electrode particles,” *Journal of Power Sources*, vol. 272, Dec. 2014, doi: 10.1016/j.jpowsour.2014.08.054.

[50] S. Son, S. Jeong, E. Kwak, J. Kim, and K.-Y. Oh, “Integrated framework for SOH estimation of lithium-ion batteries using multiphysics features,” *Energy*, vol. 238, p. 121712, Jan. 2022, doi: 10.1016/j.energy.2021.121712.

[51] J. Li, K. Adewuyi, N. Lotfi, R. G. Landers, and J. Park, “A single particle model with chemical/mechanical degradation physics for lithium ion battery State of Health (SOH) estimation,” *Applied Energy*, vol. 212, pp. 1178–1190, Feb. 2018, doi: 10.1016/j.apenergy.2018.01.011.

[52] X. Lai, C. Qin, W. Gao, Y. Zheng, and W. Yi, “A State of Charge Estimator Based Extended Kalman Filter Using an Electrochemistry-Based Equivalent Circuit Model for Lithium-Ion Batteries,” *Applied Sciences*, vol. 8, no. 9, p. 1592, Sep. 2018, doi: 10.3390/app8091592.

[53] H. Dai, X. Wei, Z. Sun, J. Wang, and W. Gu, “Online cell SOC estimation of Li-ion battery packs using a dual time-scale Kalman filtering for EV applications,” *Applied Energy*, vol. 95, pp. 227–237, Jul. 2012, doi: 10.1016/j.apenergy.2012.02.044.

[54] Y. Zou, X. Hu, H. Ma, and S. E. Li, “Combined State of Charge and State of Health estimation over lithium-ion battery cell cycle lifespan for electric vehicles,” *Journal of Power Sources*, vol. 273, Jan. 2015, doi: 10.1016/j.jpowsour.2014.09.146.

[55] H. He, R. Xiong, X. Zhang, F. Sun, and J. Fan, "State-of-charge estimation of the lithium-ion battery using an adaptive extended Kalman filter based on an improved Thevenin model," *IEEE Transactions on Vehicular Technology*, vol. 60, no. 4, pp. 1461–1469, May 2011, doi: 10.1109/TVT.2011.2132812.

[56] J. Snoussi, S. ben Elghali, M. Zerrougui, M. Bensoam, M. Benbouzid, and M. F. Mimouni, "Unknown input observer design for lithium-ion batteries SOC estimation based on a differential-algebraic model," *Journal of Energy Storage*, vol. 32, p. 101973, Dec. 2020, doi: 10.1016/J.EST.2020.101973.

[57] K. D. Rao, A. H. Chander, and S. Ghosh, "Robust Observer Design for Mitigating the Impact of Unknown Disturbances on State of Charge Estimation of Lithium Iron Phosphate Batteries Using Fractional Calculus," *IEEE Transactions on Vehicular Technology*, vol. 70, no. 4, pp. 3218–3231, Apr. 2021, doi: 10.1109/TVT.2021.3066249.

[58] J. Xu, C. C. Mi, B. Cao, J. Deng, Z. Chen, and S. Li, "The state of charge estimation of lithium-ion batteries based on a proportional-integral observer," *IEEE Transactions on Vehicular Technology*, vol. 63, no. 4, pp. 1614–1621, 2014, doi: 10.1109/TVT.2013.2287375.

[59] F. Zhong, H. Li, S. Zhong, Q. Zhong, and C. Yin, "An SOC estimation approach based on adaptive sliding mode observer and fractional order

equivalent circuit model for lithium-ion batteries," *Communications in Nonlinear Science and Numerical Simulation*, vol. 24, no. 1–3, pp. 127–144, Jul. 2015, doi: 10.1016/J.CNSNS.2014.12.015.

[60] Y. Guo, Z. Zhao, and L. Huang, "SoC Estimation of Lithium Battery Based on Improved BP Neural Network," *Energy Procedia*, vol. 105, pp. 4153–4158, May 2017, doi: 10.1016/j.egypro.2017.03.881.

[61] Z. Guo, X. Qiu, G. Hou, B. Y. Liaw, and C. Zhang, "State of health estimation for lithium ion batteries based on charging curves," *Journal of Power Sources*, vol. 249, pp. 457–462, Mar. 2014, doi: 10.1016/j.jpowsour.2013.10.114.

[62] M. A. Awadallah and B. Venkatesh, "Accuracy improvement of SOC estimation in lithium-ion batteries," *Journal of Energy Storage*, vol. 6, May 2016, doi: 10.1016/j.est.2016.03.003.

[63] J. Chen, Q. Ouyang, C. Xu, and H. Su, "Neural Network-Based State of Charge Observer Design for Lithium-Ion Batteries," *IEEE Transactions on Control Systems Technology*, vol. 26, no. 1, pp. 313–320, Jan. 2018, doi: 10.1109/TCST.2017.2664726.

[64] C. Chen, R. Xiong, R. Yang, W. Shen, and F. Sun, "State-of-charge estimation of lithium-ion battery using an improved neural network model and extended Kalman filter," *Journal of Cleaner Production*,

vol. 234, pp. 1153–1164, Oct. 2019, doi: 10.1016/j.jclepro.2019.06.273.

[65] W. He, N. Williard, C. Chen, and M. Pecht, "State of charge estimation for Li-ion batteries using neural network modeling and unscented Kalman filter-based error cancellation," *International Journal of Electrical Power & Energy Systems*, vol. 62, pp. 783–791, Nov. 2014, doi: 10.1016/j.ijepes.2014.04.059.

[66] X. Dang, L. Yan, K. Xu, X. Wu, H. Jiang, and H. Sun, "Open-Circuit Voltage-Based State of Charge Estimation of Lithium-ion Battery Using Dual Neural Network Fusion Battery Model," *Electrochimica Acta*, vol. 188, pp. 356–366, Jan. 2016, doi: 10.1016/J.ELECTACTA.2015.12.001.

[67] Y. Boujoudar, H. Elmoussaoui, and T. Lamhamdi, "Lithium-Ion batteries modeling and state of charge estimation using Artificial Neural Network," *International Journal of Electrical and Computer Engineering (IJECE)*, vol. 9, no. 5, p. 3415, Oct. 2019, doi: 10.11591/ijece.v9i5.pp3415-3422.

[68] M. Wei, M. Ye, J. B. Li, Q. Wang, and X. X. Xu, "State of charge estimation for lithium-ion batteries using dynamic neural network based on sine cosine algorithm," *Proceedings of the Institution of Mechanical Engineers, Part D: Journal of Automobile Engineering*,

vol. 236, no. 2–3, pp. 241–252, Feb. 2022, doi: 10.1177/09544070211018038.

[69] W. He, N. Williard, C. Chen, and M. Pecht, "State of charge estimation for Li-ion batteries using neural network modeling and unscented Kalman filter-based error cancellation," *International Journal of Electrical Power & Energy Systems*, vol. 62, pp. 783–791, Nov. 2014, doi: 10.1016/J.IJEPES.2014.04.059.

[70] Z. Deng, X. Hu, X. Lin, Y. Che, L. Xu, and W. Guo, "Data-driven state of charge estimation for lithium-ion battery packs based on Gaussian process regression," *Energy*, vol. 205, p. 118000, Aug. 2020, doi: 10.1016/j.energy.2020.118000.

[71] D. P. Abraham, E. M. Reynolds, E. Sammann, A. N. Jansen, and D. W. Dees, "Aging characteristics of high-power lithium-ion cells with LiNi0.8Co0.15Al0.05O2 and Li4/3Ti5/3O4 electrodes," *Electrochimica Acta*, vol. 51, no. 3, Oct. 2005, doi: 10.1016/j.electacta.2005.05.008.

[72] D. Zhang, L. D. Couto, and S. J. Moura, "Electrode-Level State Estimation in Lithium-Ion Batteries via Kalman Decomposition," *IEEE Control Systems Letters*, vol. 5, no. 5, Nov. 2021, doi: 10.1109/LCSYS.2020.3042751.

[73] W. Li *et al.*, "Physics-informed neural networks for electrode-level state estimation in lithium-ion batteries," *Journal of Power Sources*, vol. 506, p. 230034, Sep. 2021, doi: 10.1016/J.JPOWSOUR.2021.230034.

[74] S. Lee, J. B. Siegel, A. G. Stefanopoulou, J.-W. Lee, and T.-K. Lee, "Electrode State of Health Estimation for Lithium Ion Batteries Considering Half-cell Potential Change Due to Aging," *Journal of The Electrochemical Society*, vol. 167, no. 9, Jan. 2020, doi: 10.1149/1945-7111/ab8c83.

[75] E. McTurk, C. R. Birkl, M. R. Roberts, D. A. Howey, and P. G. Bruce, "Minimally Invasive Insertion of Reference Electrodes into Commercial Lithium-Ion Pouch Cells," *ECS Electrochemistry Letters*, vol. 4, no. 12, pp. A145–A147, Nov. 2015, doi: 10.1149/2.0081512eel.

[76] L. Somerville, S. Ferrari, M. Lain, A. McGordon, P. Jennings, and R. Bhagat, "An In-Situ Reference Electrode Insertion Method for Commercial 18650-Type Cells," *Batteries*, vol. 4, no. 2, Apr. 2018, doi: 10.3390/batteries4020018.

[77] F. J. Vidal-Iglesias, J. Solla-Gullón, A. Rodes, E. Herrero, and A. Aldaz, "Understanding the Nernst Equation and Other Electrochemical Concepts: An Easy Experimental Approach for Students," *Journal of*

Chemical Education, vol. 89, no. 7, pp. 936–939, Jun. 2012, doi: 10.1021/ed2007179.

[78] Z. S. Zu, "Generalized Chi Square Method for the Estimation of Weights," *Journal of Optimization Theory and Applications*, vol. 107, no. 1, pp. 183–192, Oct. 2000, doi: 10.1023/A:1004617102663.

[79] B. R. Dewangga, S. Herdjunanto, and A. Cahyadi, "Unknown Input Observer for Battery Open Circuit Voltage Estimation: an LMI Approach," in *2018 10th International Conference on Information Technology and Electrical Engineering (ICITEE)*, Jul. 2018, pp. 471–475. doi: 10.1109/ICITEED.2018.8534889.

[80] S. Nazari, "The Unknown Input Observer and its Advantages with Examples," Apr. 2015.

[81] M. Darouach, M. Zasadzinski, and S. J. Xu, "Full-order observers for linear systems with unknown inputs," *IEEE Transactions on Automatic Control*, vol. 39, no. 3, pp. 606–609, Mar. 1994, doi: 10.1109/9.280770.

[82] Weitian Chen and M. Saif, "Unknown input observer design for a class of nonlinear systems: an LMI approach," in *2006 American Control Conference*, 2006, p. 5 pp. doi: 10.1109/ACC.2006.1655461.

[83] H. He, R. Xiong, and J. Fan, "Evaluation of Lithium-Ion Battery Equivalent Circuit Models for State of Charge Estimation by an

Experimental Approach," *Energies (Basel)*, vol. 4, no. 4, pp. 582–598, Mar. 2011, doi: 10.3390/en4040582.

[84] J. Chen, R. Wang, Y. Li, and M. Xu, "A Simplified Extension of Physics-Based Single Particle Model for Dynamic Discharge Current," *IEEE Access*, vol. 7, pp. 186217–186227, 2019, doi: 10.1109/ACCESS.2019.2961509.